

CONDUCTOR AND DIELECTRIC PROPERTY EXTRACTION USING MICROSTRIP TEE
RESONATORS

Except where reference is made to the work of others, the work described in this thesis is my own or was done in collaboration with my advisory committee. This thesis does not include proprietary or classified information.

Andrew Richard Fulford

Certificate of Approval:

Lloyd S. Riggs
Professor
Electrical and Computer Engineering

Stuart M. Wentworth, Chair
Associate Professor
Electrical and Computer Engineering

R. Wayne Johnson
Samuel Ginn Distinguished Professor
Electrical and Computer Engineering

Stephen L. McFarland
Dean
Graduate School

CONDUCTOR AND DIELECTRIC PROPERTY EXTRACTION USING MICROSTRIP TEE
RESONATORS

Andrew Richard Fulford

A Thesis

Submitted to

the Graduate Faculty of

Auburn University

in Partial Fulfillment of the

Requirements for the

Degree of

Master of Science

Auburn, Alabama
August 8, 2005

CONDUCTOR AND DIELECTRIC PROPERTY EXTRACTION USING MICROSTRIP TEE
RESONATORS

Andrew Richard Fulford

Permission is granted to Auburn University to make copies of this thesis at its discretion,
upon the request of individuals or institutions and at their expense. The author reserves
all publication rights.

Signature of Author

Date

Copy sent to:

Name _____ Date _____

VITA

Andrew Richard Fulford, son of Charles Richard Fulford and Burdette Hughes, was born February 28, 1979 in Enterprise, Alabama. He graduated from Enterprise High School in 1997. For the next two years he was enrolled at Enterprise State Junior College before transferring to Auburn University's engineering program in the Fall of 1999. He completed a co-op program with Milliken and Company and an internship with the Army Aviation Technical Testing Center during his undergraduate studies at Auburn University. In May of 2003 he received a Bachelor's of Electrical Engineering. He continued his education becoming a graduate student in the Department of Electrical and Computer Engineering at Auburn University. While completing his graduate degree, his research effort has been in the area of microwave material characterization.

THESIS ABSTRACT
CONDUCTOR AND DIELECTRIC PROPERTY EXTRACTION USING MICROSTRIP TEE
RESONATORS

Andrew Richard Fulford

Master of Science, August 8, 2005
(B.E.E., Auburn University, 2003)

95 Typed Pages

Directed by Stuart M. Wentworth

The growth and resultant competitive nature of the wireless industry has prompted the need for high frequency electronics to be provided at a low cost. An efficient method of component characterization is necessary to ensure that circuit designs meet the specifications for desired performance in as few design iterations as possible. The use of board “real estate” is also a consideration in the choice of a test structure to be used for component characterization. The open-ended quarter wave tee resonator in a microstrip configuration is such a test structure.

This thesis describes a method using tee resonator measurements to extract line attenuation and further to extract dielectric relative permittivity and loss tangent if the characteristics of the conductor are assumed. Furthermore, a novel approach is presented where a pair of microstrip tee resonators are employed, each with a different impedance

resonating element, and the behavior of the resonances is used to extract conductor sheet resistance as well as the dielectric properties. The method is demonstrated for screen-printed silver epoxy lines on an alumina substrate. This methodology is further examined by way of method of moments modeling. This modeling is used to validate the procedure that was developed for use on physical test boards.

ACKNOWLEDGEMENTS

The author would like to express his sincere appreciation to his family for providing continued love and support and for their patience throughout his life. To his advisor, Dr. Stuart M. Wentworth, the author would like to sincerely thank him for the opportunity to study under him and for patience, guidance, and selflessness throughout the years of study. The author appreciates Mr. Mike Palmer and Mr. Joe Haggerty for their guidance and assistance in the board fabrication efforts. The author wishes to acknowledge the assistance and support of the Alabama Microelectronics Science and Technology Center and the Auburn University Information Technology Peak of Excellence. Lastly, the author would like to thank everyone who helped make his time at Auburn University a productive and enjoyable one.

Style manual of journal used Graduate School: Guide to preparation and submission of theses and dissertations

Computer software used Microsoft Office 2003, Matlab 6.0, ADS, Flowmerics Micro-Stripes 6.0

TABLE OF CONTENTS

LIST OF TABLES.....	xi
LIST OF FIGURES.....	xii
CHAPTER 1: INTRODUCTION.....	1
1.1 Motivation	1
1.2 Test structures.....	2
1.2.1 Scattering parameter tutorial.....	2
1.2.2 Meander lines.....	5
1.2.3 Gap-coupled resonator.....	6
1.2.4 Open-ended stub tee resonator.....	7
1.3 Presented technique.....	8
CHAPTER 2: PROPERTY EXTRACTION APPROACH.....	10
2.1 Operation of tee resonator.....	10
2.2 Permittivity and attenuation extraction.....	12
2.3 Dielectric and conductor property extraction.....	18
CHAPTER 3: BOARD FABRICATION.....	23
3.1 Fabrication.....	23
CHAPTER 4: MEASUREMENTS.....	31
4.1 Measurement procedure.....	31
4.1.1 Standard procedure.....	32
4.1.2 Variability study.....	35
4.2 Property extraction.....	37
4.2.1 Permittivity extraction.....	37
4.2.2 Total attenuation extraction.....	40
4.2.3 Sheet resistance and loss tangent extraction.....	43
CHAPTER 5: SIMULATION.....	45
5.1 Board design verification.....	45
5.2 Modeling approach.....	47
5.2.1 ADS “momentum”.....	48
5.2.2 Flowmerics micro-stripes.....	48
5.2.3 Property extraction verification approach.....	49
5.3 Results.....	51

5.3.1 Model meshing resolution.....	51
5.3.2 Delta L calculation.....	53
5.3.3 Relative permittivity extraction.....	55
5.3.4 Sheet resistance and loss tangent extraction.....	57
CHAPTER 6: CONCLUSIONS.....	61
6.1 Technique summary.....	61
6.2 Future work.....	62
6.3 Conclusions.....	64
REFERENCES.....	65
APPENDIX: MATLAB CODE	68
1 Plot of sheet resistance versus loss tangent code.....	68
2 Code for extracting the resonant frequency for the first line.....	71
3 Effective permittivity calculation code.....	71
4 Characteristic impedance calculation code.....	73
5 Code for calculating total attenuation for the first line.....	73
6 Relative permittivity calculation code.....	75
7 Code used in the permittivity calculation.....	76
8 Code used to compute ΔL	76
9 Code for the calculation of attenuation due to radiation.....	77
10 Sheet resistance calculation code.....	77
11 Conductor attenuation calculation code.....	78
12 Code for extracting the resonant frequency for the second line.....	79
13 Code for calculating total attenuation for the second line.....	80

LIST OF TABLES

3.1	Tee resonator and calibration line design dimensions.....	23
4.1	Average value and standard deviation of total attenuation with and without using TDR to place the probes	35
4.2	Measurement variability.....	36
4.3	Typical data for the test board.....	38
4.4	Typical permittivity extraction results.....	38
4.5	Typical total attenuation extraction results.....	41
4.6	Interpolation addition results.....	42
5.1	Results of delta L experiment.....	54
5.2	Design parameters for model set.....	56
5.3	Extracted relative permittivity and resonant frequency values.....	57

LIST OF FIGURES

1.1	Two-port network.....	2
1.2	Two-port scattering matrix description.....	3
1.3	Two-port network terminated in a matched load.....	4
1.4	Meander lines.....	5
1.5	Gap-coupled resonator.....	7
1.6	Open-ended stub tee resonator.....	8
2.1	Basic illustration of the microstrip tee resonator.....	10
2.2	Diagram indicating the 2 ports and the point of input impedance.....	11
2.3	Resonant S_{21} dips for the tee resonator.....	12
2.4	Cross-section of microstrip line.....	13
2.5	The S_{21} measurement at a resonant dip for a tee resonator.....	13
2.6	Permittivity calculation flowchart.....	16
2.7	Total attenuation calculation flowchart.....	17
2.8	Extraction of R_S and $\tan\delta$ flowchart.....	21
2.9	Ideal intersection plot for a pair of tee resonators that shows how $\tan\delta$ and R_S are extracted.....	22
3.1	Lavenir layout for tee resonators and calibration line.....	24
3.2	Mask for tee resonators and calibration through line.....	25
3.3	Screens for the resonators and groundplane.....	26
3.4	Screenprinter.....	27

3.5	Drying oven.....	28
3.6	Firing oven.....	28
3.7	Completed microstrip tee resonator test structure.....	29
4.1	Probe in contact with board during testing.....	31
4.2	Testing equipment.....	32
4.3	Test board during measurement on the Alessi probe station.....	33
4.4	TDR signatures of correct and incorrect probe placement.....	34
4.5	Plot of long 30 ohm resonator relative permittivity vs. long 50 ohm resonator relative permittivity.....	39
4.6	Single dip used for attenuation calculation.....	40
4.7	Chart comparison of 30-sample study of long 50 Ω tee resonator with (black) and without (grey) the MATLAB interpolation addition.....	42
4.8	Plot of sheet resistance vs. loss tangent using measurements on a 30 Ω and 50 Ω tee resonator pair.....	43
5.1	ADS schematic layout used in the design of the test board.....	46
5.2	Resonant dips used for confirmation of the design of the four resonators.....	47
5.3	Property extraction verification approach using modeling.....	50
5.4	Progression of resonant frequency towards target value using micro-stripes.....	51
5.5	Progression of resonant frequency towards target value using ADS “momentum”.....	52
5.6	Definition of resonator length with consideration of ΔL	53
5.7	Extraction of relative permittivity.....	55
5.8	300 cells per wavelength sheet resistance vs. loss tangent plot.....	58
5.9	500 cells per wavelength sheet resistance vs. loss tangent plot.....	59
5.10	700 cells per wavelength sheet resistance vs. loss tangent plot.....	60

6.1 Sheet resistance vs. loss tangent plot for test board with copper lines and a microwave laminate substrate.....63

CHAPTER 1

INTRODUCTION

1.1 Motivation

The emergence of wireless communications has prompted the need for cheap and reliable microwave and rf circuit components. This need is evident in both commercial and military applications. For example, wireless local area networks (LAN)'s rely on high frequency circuitry to provide service for data communication in the commercial and military environment. Another example is the demand for inexpensive but robust circuitry in the cellular phone industry. The ability to provide reliable microwave and rf circuitry while observing a low manufacturing cost is of utmost importance due to the competitive nature of these markets. In order to keep manufacturing costs at a minimum it is important for high frequency designers to have accurate characterization of the components used in the circuit design. This will lessen the number of costly manufacturing iterations required to reach the level of performance that is desired from the circuit, thus lowering overall manufacturing cost. The wide variety of substrates and metallizations in use and projected for use in microwave and rf circuits drives the need for accurate microstrip loss measurements. In many cases, it is difficult to accurately model losses because of uncertainties in surface roughness and in the behavior of the dielectrics as a function of frequency or environmental conditions [1,2].

1.2 Test structures

A number of test structures have been developed to measure the line attenuation of microstrip circuits [3-6]. Three commonly used test structures are meander lines, gap-coupled resonators, and open-ended stub tee resonators. The advantages and disadvantages of these test structures will be discussed in the following sections. A brief tutorial in scattering parameters will first be given to serve as an aid in the comprehension of the following discussions.

1.2.1 Scattering parameter tutorial

Scattering parameters (S-parameters) and the associated scattering matrix can be used to characterize multiport networks at high frequencies [7]. Scattering matrices are viewed as a representation more in accord with actual measurements because they deal with the principles of incident, reflected, and transmitted waves [8]. This concept is important because the measurements taken with a network analyzer in this work are best explained by the concept of scattering parameters.

Consider a device of the type shown in Figure 1.1. Here, the device is commonly referred to as a two port network. It is important to note that the scattering matrix can be

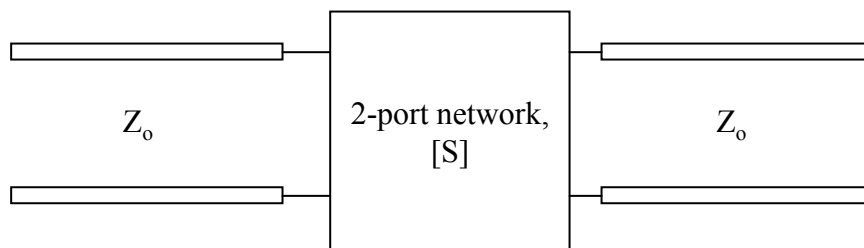


Figure 1.1 Two-port network

formed for a network possessing more than 2 ports. But, for the purposes of this work, only an understanding of a two port network is required. This two port network can be used to represent the ratios of voltage amplitude entering and leaving a port as shown in Figure 1.2. Upon observation, it is evident that V_1^- is composed of the portion of V_1^+ that is reflected and the portion of V_2^+ that is transmitted. This behavior can be written in terms of the scattering parameters as

$$V_1^- = S_{11}V_1^+ + S_{12}V_2^+ . \quad (1.1)$$

V_2^- can be written in a similar fashion as

$$V_2^- = S_{21}V_1^+ + S_{22}V_2^+ . \quad (1.2)$$

These expressions can then be expressed in the matrix form as

$$\begin{bmatrix} V_1^- \\ V_2^- \end{bmatrix} = \begin{bmatrix} S_{11} & S_{12} \\ S_{21} & S_{22} \end{bmatrix} \begin{bmatrix} V_1^+ \\ V_2^+ \end{bmatrix} . \quad (1.3)$$

A particular scattering parameter, S_{ij} , can be defined as the fraction of the voltage wave entering port j that exits port i [7]. This can be written in general terms as

$$S_{ij} = \left. \frac{V_i^-}{V_j^+} \right|_{V_k^+ = 0, k \neq j} . \quad (1.4)$$

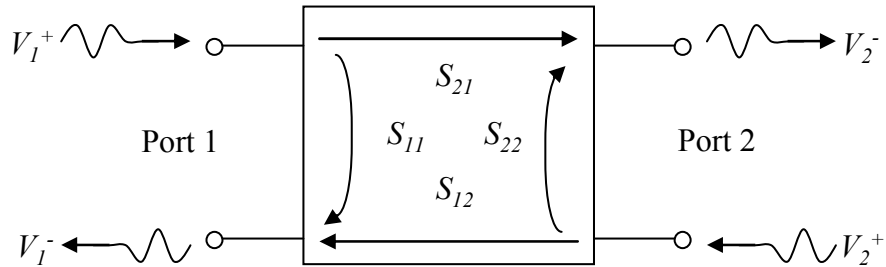


Figure 1.2 Two-port scattering matrix description

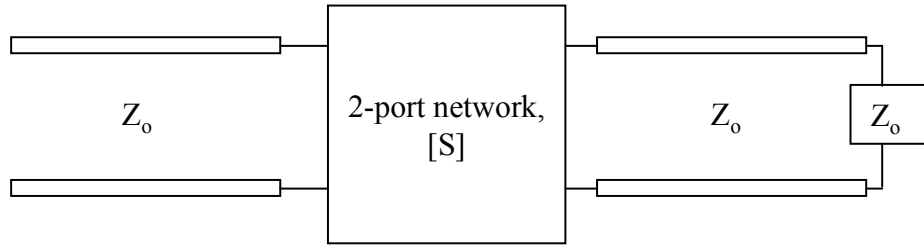


Figure 1.3 Two-port network terminated in a matched load

This can also be thought of as the source of the voltage being at the j^{th} port and the destination of the voltage being at the i^{th} port.

We can determine the transmission scattering matrix, S_{21} , by terminating port 2 in a matched load as shown in Figure 1.3. This will result in $V_2^+ = 0$ and the resultant S-parameter is

$$S_{21} = \left. \frac{V_2^-}{V_1^+} \right|_{V_2^+ = 0}. \quad (1.5)$$

The scattering parameter, S_{21} , is most commonly used in this work to represent the amount of power transferred from port 1 to port 2 during the measurement procedure. This translation of S_{21} into a form of power listed in units of dB can be performed by multiplying the log magnitude of S_{21} by 20:

$$S_{21}(dB) = 20 \log \left| \frac{V_2^-}{V_1^+} \right|. \quad (1.6)$$

$$S_{21}(dB) = 20 \log |S_{21}|$$

1.2.2 Meander lines

Meander lines are two different length transmission lines that meander across the surface of the substrate as illustrated in Figure 1.4. Attenuation in microstrip line is found by taking the difference in the measured log magnitude of the scattering parameter S_{21} for two different length meandering transmission lines [9]. This method is useful in removing losses associated with induced discontinuities such as ports and connectors [5]. A method of calculating the total attenuation in terms of decibels per unit length involves dividing the difference in the S_{21} log magnitude data by the difference of the two line lengths. This method requires that the impedance of the lines used closely match the testing equipment impedance (50Ω). Otherwise, standing waves established in the lines will overwhelm the difference data. With this approach it is often necessary to apply averaging techniques on the data to ensure accuracy in the extraction procedure due to the characteristic ripple of the measured data [5]. Smoothing, a linearly moving average of adjacent points, is often used to remove some of the ripple in the data during measurement. It is important to note that smoothing is applied to the line measurement rather than to the difference data since the ripple is a function of line length. Smoothing

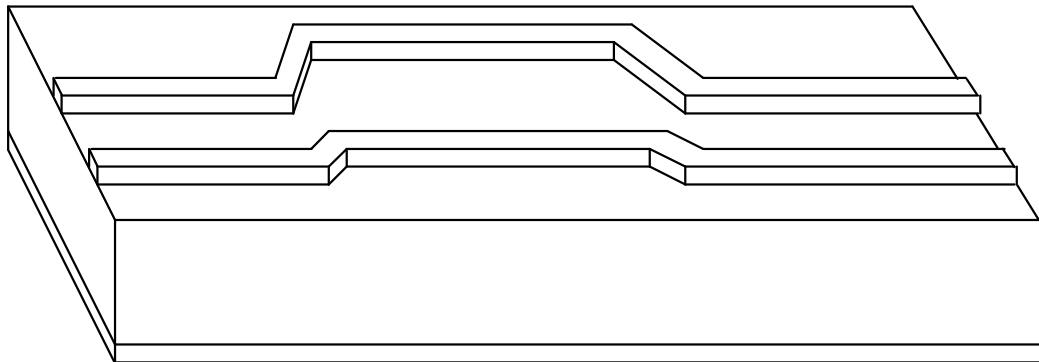


Figure 1.4 Meander lines

must be used carefully as to not mask the true behavior at low frequency ranges [9].

1.2.3 *Gap-coupled resonator*

A gap-coupled resonator is essentially a structure consisting of a transmission line separated by gaps on either side. A diagram depicting the typical microstrip gap-coupled resonator structure is shown in Figure 1.5. The property extraction approach involves measuring the resonant S_{21} peaks that occur when the resonator length is integral multiples of a half guide wavelength [5]. These peaks are used to find the quality factor. This quality factor can then be used to compute total attenuation. This type of resonator exhibits the most productive measurements with low loss lines [5,3]. This is in contrast to the meander line approach. Care in the collection of S_{21} measurement data must be exercised due to the nature of the resonant peaks. This method requires that measurements be taken with a frequency span in close proximity to the peak of interest to allow a high resolution of the collected data. This high resolution of collected data helps to ensure an accurate calculation for attenuation. It is also apparent that this type of test structure is susceptible to capacitive loading at the gaps. This behavior leads to increased resonator electrical length and subsequent inaccuracy in the extracted properties at high frequencies [4].

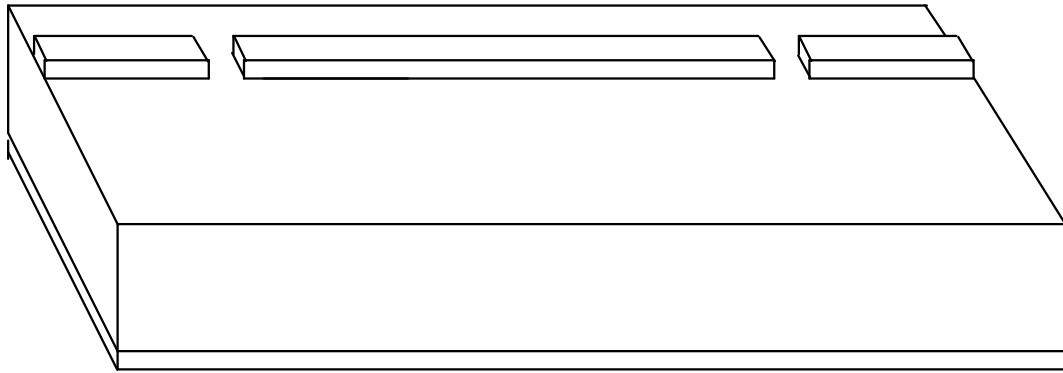


Figure 1.5 Gap-coupled resonator

1.2.4 *Open-ended stub tee resonator*

Tee resonators have been used to determine the relative permittivity and loss tangent of dielectric substrates when the conductor properties were known [4,6,10]. A diagram depicting a typical tee resonator microstrip test structure is shown in Figure 1.6. The basic principal is that an open-ended transmission line stub appears as a short circuit at periodic frequencies. Transmission measurements reveal resonant dips at these frequencies. The resonant frequencies are used to extract relative permittivity, while the quality factor of the dips is used to extract line attenuation. The collected data has been touted as being more accurate than a gap-coupled half-wavelength resonator because there is one open end for radiative loss instead of four open ends [4,6].

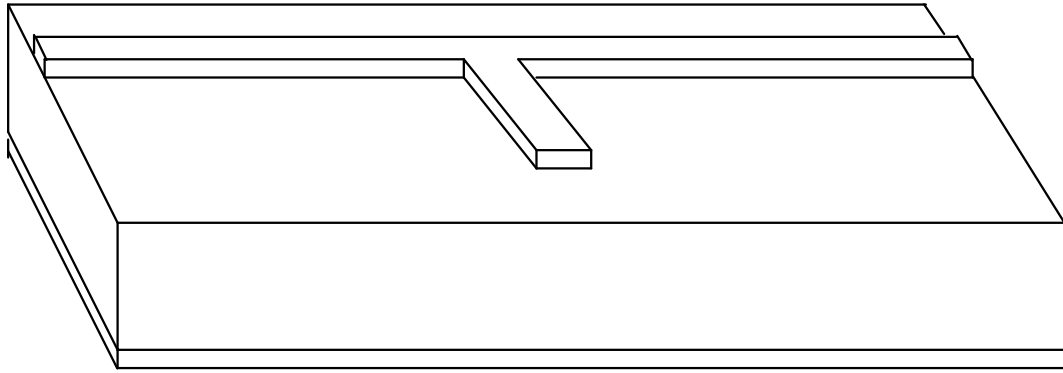


Figure 1.6 Open-ended stub tee resonator

1.3 Presented technique

In this work a technique is presented for the extraction of the permittivity and loss tangent of the substrate and the sheet resistance of the conductor using the open-ended tee resonator structure. The total line attenuation consists of conductor, dielectric and radiative loss. The radiative loss is a small but appreciable component that can be calculated at the frequency range of interest [11,12]. The dielectric loss is a function of loss tangent, while the conductor loss is a function of metal conductivity and roughness at the conductor-dielectric interface. Both types are also a function of line geometry. It is common practice to assume the conductor properties in order to estimate the dielectric properties [3,6]. But since the attenuation is often dominated by conductor loss, small error in the assumed conductor properties can result in large errors in the extracted loss tangent.

For both the through line and the open-ended stub of a tee line resonator, the characteristic impedance is customarily chosen to match the system impedance (e.g. 50

Ω). But the open-ended stub will present resonant frequency dips regardless of its characteristic impedance. Because the losses are also a function of line dimensions, different width stubs will have attenuations consisting of different contributions from conductor and dielectric loss. The method proposed in this work describes how measurements on a pair of tee resonators can be used to extract both conductor sheet resistance and the dielectric loss tangent. The method is demonstrated for screen-printed Ag/Pd microstrip lines on an alumina substrate. An interesting result is that the extraction approach did not work as well as expected. This may be a result of the dated equations used in the process, minor flaws in the board preparation, or inaccuracies in the extraction routine itself. Method of moments modeling was used in an effort to understand why the approach was not as accurate as expected.

CHAPTER 2

PROPERTY EXTRACTION APPROACH

2.1 Operation of tee resonator

The quarter wavelength open ended tee resonator is presented in the microstrip configuration as shown in Figure 2.1. The tee resonator test structure is formed by a dielectric material sandwiched between a conductor in the form of a tee on top and a groundplane conductor covering the bottom surface of the dielectric. This complete structure forms the microstrip tee resonator test vehicle. The conductor forming the tee

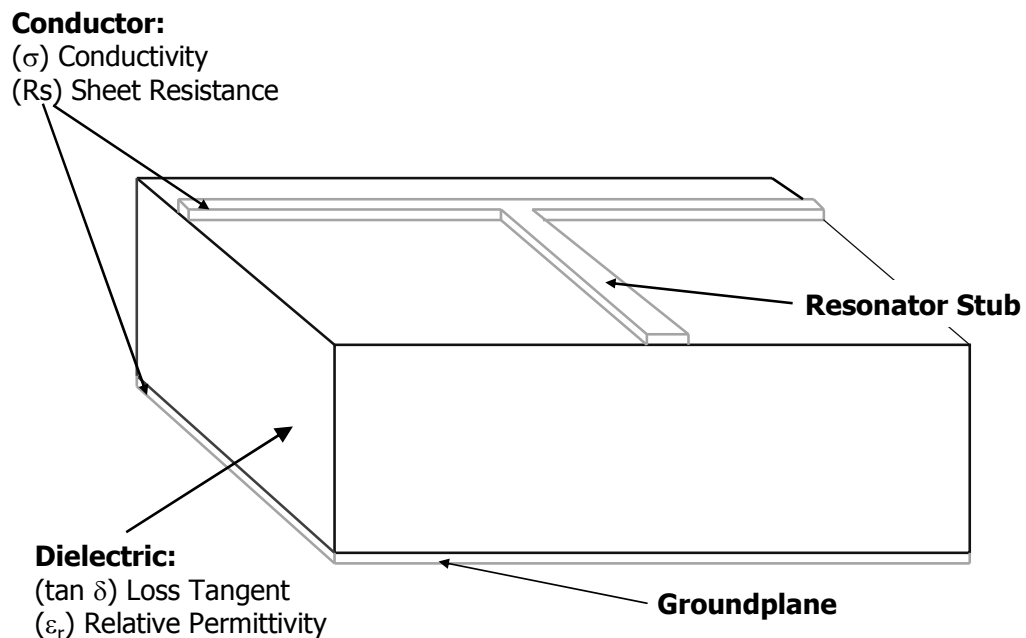


Figure 2.1 Basic illustration of the microstrip tee resonator

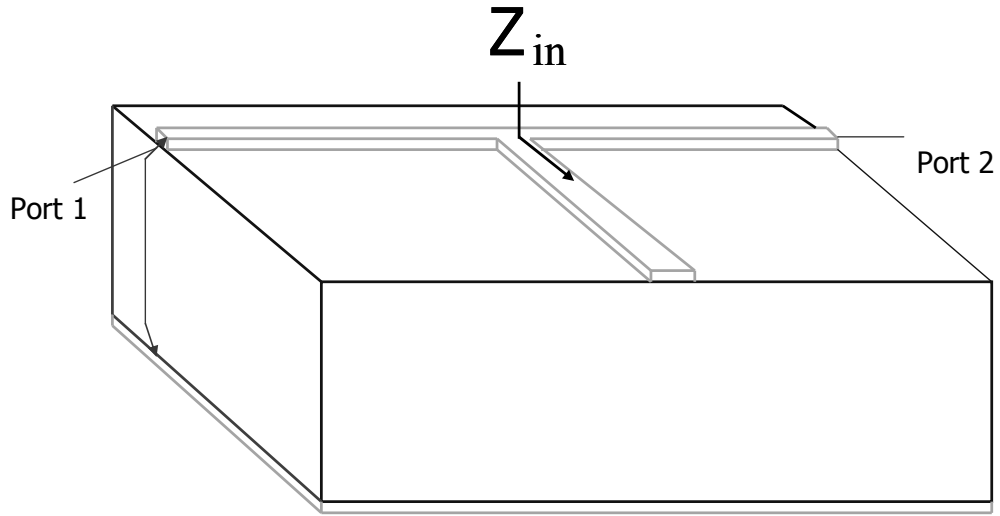


Figure 2.2 Diagram indicating the 2 ports and the point of input impedance

and the groundplane possess the associated parameters conductivity and sheet resistance. The dielectric material has the associated parameters loss tangent and relative permittivity.

The tee resonator ideally appears as an electrical short circuit at the frequency where the stub is one quarter wavelength long. This behavior is observed by computing the impedance looking into the stub of the tee resonator as indicated in Figure 2.2. This characteristic can be expressed by evaluating the input impedance Z_{in} [13]:

$$Z_{in} = Z_0 \frac{Z_L + jZ_0 \tan \beta l}{Z_0 + jZ_L \tan \beta l} \quad \left(\text{where } \beta = \frac{2\pi}{\lambda} \right). \quad (2.1)$$

For the quarter wavelength stub we have $l = \frac{\lambda}{4}$, so $\tan \beta l = \tan\left(\frac{\pi}{2}\right) = \infty$. Inserting this

result into (2.1) gives $Z_{in} = Z_0 \frac{jZ_0}{jZ_L} = \frac{Z_0^2}{Z_L}$. Now, since the stub is open-ended, Z_L appears

infinite, so $Z_{in} = \frac{Z_0^2}{\infty} = 0$. No power would be transferred from port 1 to port 2 in this

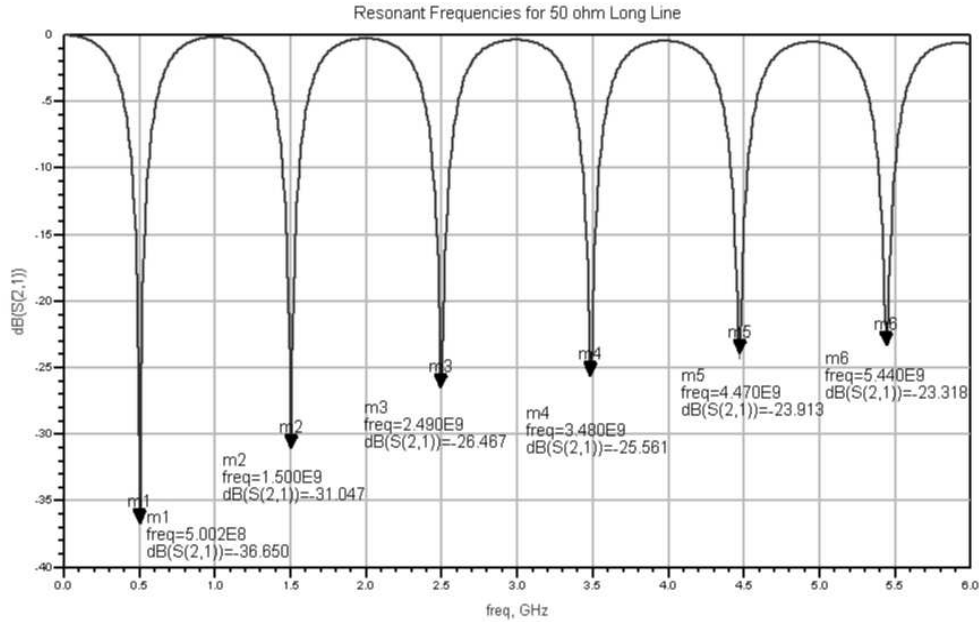


Figure 2.3 Resonant S_{21} dips for the tee resonator

ideal case. But because of losses, the line does not quite appear as a perfect short, and sharp dips in the measured transmitted power (S_{21}) occur at the resonant frequency and at integer multiples of a half wavelength higher in frequency. An example of the dips caused by this characteristic behavior is shown in Figure 2.3.

2.2 Permittivity and attenuation extraction

Consider a microstrip line with dimensions shown in the Figure 2.4 cross section. Here, the metal is characterized as having a conductivity, σ , and the dielectric has a loss tangent, $\tan\delta$. In Figure 2.5, the frequency-dependent parameter S_{21} corresponds to the transmitted power from port 1 to port 2 of the tee resonator (inset).

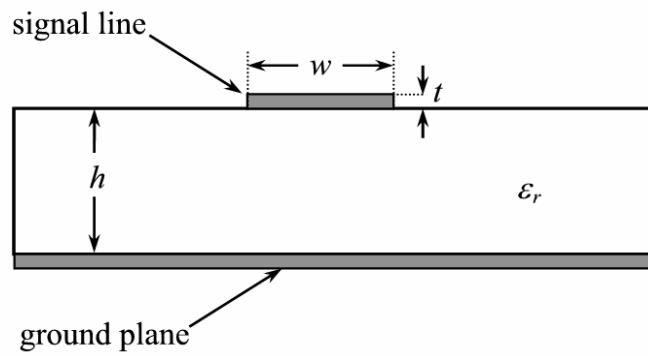


Figure 2.4 Cross-section of microstrip line

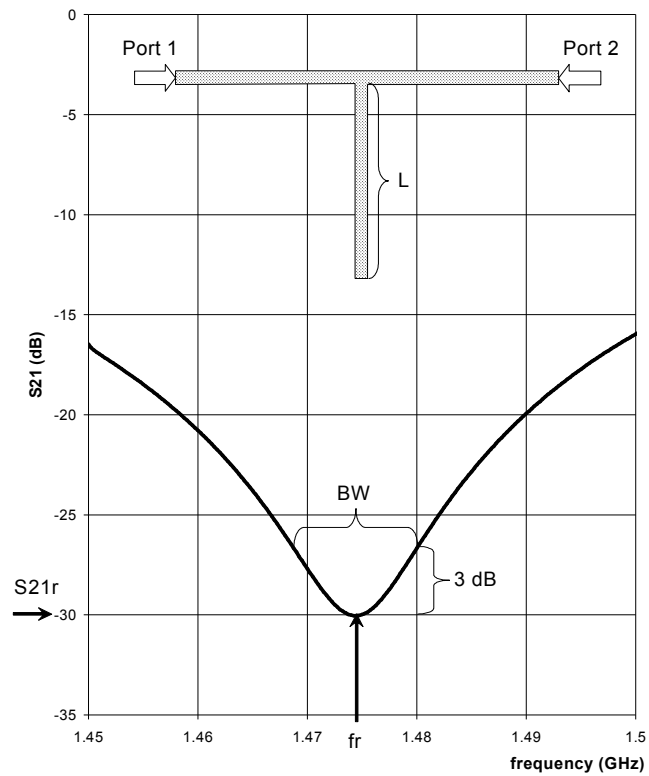


Figure 2.5 The S_{21} measurement at a resonant dip for a tee resonator

The guide wavelength λ_G is related to the length of the stub L at a resonance condition by

$$L + \Delta L = \frac{[2(N-1)+1]\lambda_G}{4}, \quad (2.2)$$

where $N = 1, 2, 3, \dots$ and is termed the resonance number. Here, $N = 1$ corresponds to the fundamental resonance where the stub length is equal to a quarter of a guide wavelength. For a nonmagnetic material the guide wavelength is related to resonance frequency and the effective relative permittivity ϵ_e by [14]

$$\lambda_G = \frac{c}{f_r \sqrt{\epsilon_e}}. \quad (2.3)$$

Manipulation of (2.4) and (2.5) yields

$$\epsilon_e = \left[\frac{(2N-1)c}{4f_r(L + \Delta L)} \right]^2. \quad (2.4)$$

The correction length ΔL is a small but appreciable length resulting from fringing fields at the open end of the microstrip stub. It can be estimated using the approach of Kirshchning *et al* [15]:

$$\Delta L = \frac{k_1 k_3 k_6}{k_5} h, \quad (2.5)$$

where

$$k_1 = 0.434907 \left(\frac{\epsilon_e^{0.81+0.26}}{\epsilon_e^{0.81}-0.189} \right) \left(\frac{\left(\frac{w}{h} \right)^{0.8544} + 0.236}{\left(\frac{w}{h} \right)^{0.8544} + 0.87} \right)$$

$$k_2 = 1 + \frac{\left(\frac{w}{h}\right)^{0.371}}{2.358\varepsilon_r + 1}$$

$$k_3 = 1 + \frac{0.5274 \tan^{-1} \left[0.084 \left(\frac{w}{h}\right)^{1.9413/k_2} \right]}{\varepsilon_e^{0.9236}}$$

$$k_4 = 0.0377 \left(6 - 5e^{0.036(1-\varepsilon_r)} \right)$$

$$k_5 = 1 + k_4 \tan^{-1} \left[0.067 \left(\frac{w}{h}\right)^{1.456} \right]$$

$$k_6 = 1 - 0.218e^{-7.5w/h}.$$

If ε_e is known, then ε_r can be calculated using more complex equations that fit numerical quasi-static solutions within 0.2% [16].

$$\varepsilon_e = \frac{\varepsilon_r + 1}{2} + \frac{\varepsilon_r - 1}{2} (1 + 10h/w)^{-ab} \quad (2.6)$$

$$\text{where } b = 0.564 \left(\frac{\varepsilon_r + 0.9}{\varepsilon_r + 3} \right)^{0.053} \text{ and}$$

$$a = 1 + \left(\frac{1}{49} \right) \ln \left(\frac{\left(\frac{w}{h}\right)^4 + \left(\frac{w}{52h}\right)^2}{\left(\frac{w}{h}\right)^4 + 0.432} \right) + \left(\frac{1}{18.7} \right) \ln \left(1 + \left(\frac{w}{18.1h}\right)^3 \right)$$

It is apparent that since an accurate calculation of ε_e requires ΔL be known, and the calculation of ΔL requires both ε_e and ε_r be known, an iterative procedure must be used to find ε_e , ε_r , and ΔL . This iterative procedure is shown in Figure 2.6. First, an initial value of $\Delta L = 0$ is assumed and (2.4) is solved for ε_e . Next, this value of ε_e is used with equation (2.6) to determine ε_r . Then, the Kirschning approach (2.5) is used to find ΔL . ΔL is inserted into (2.4) to calculate a new ε_e and so on until the changes in ε_e , ε_r and ΔL are insignificant. This has only taken a few iterations in our trials.

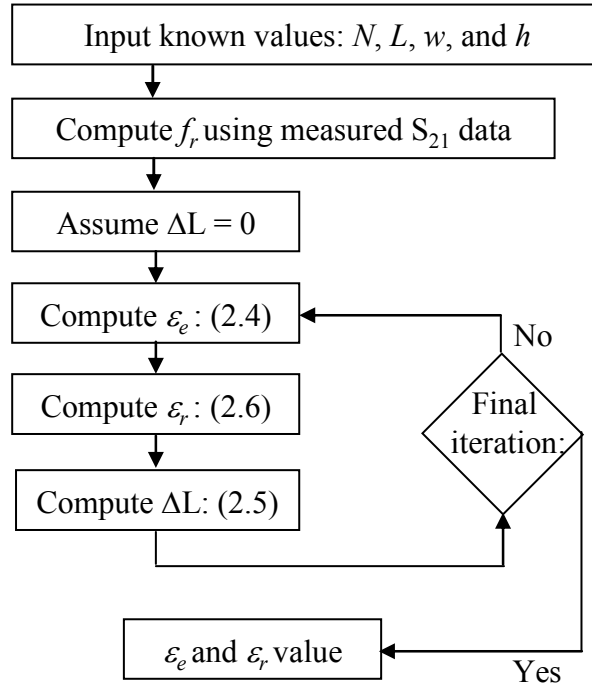


Figure 2.6 Permittivity calculation flowchart

The quality factor, or Q , provides a measure of energy loss in a resonator. The loaded quality factor Q_L is found from the BW_{3dB} and the resonance frequency f_r by [4]

$$Q_L = \frac{f_r}{BW_{3dB}}. \quad (2.7)$$

The unloaded quality factor Q_u is [4]

$$Q_U = \frac{Q_L}{\sqrt{1 - (2)10e^{((S_{21r} - S_{21t})/10)}}}. \quad (2.8)$$

Here, S_{21r} is the value of S_{21} , in dB, at the resonance frequency. S_{21t} is the transmission parameter for an equivalent length microstrip line without the tee stub. Subtracting this

term from S_{21r} in (dB) therefore corrects for losses in the through line. In practice, S_{21l} is accounted for in the calibration and can therefore be left out of the equation. For low loss lines, the loaded and unloaded Q-factors are approximately equal.

With an accurate determination of ϵ_e , we can relate the total attenuation to the unloaded Q-factor by [4]

$$\alpha_T(\text{dB}/m) = \frac{8.686\pi f_r \sqrt{\epsilon_e}}{cQ_u}. \quad (2.9)$$

A summary for the process of computing total attenuation for a given line at the resonance mode, N, is described by the flowchart indicated in Figure 2.7. Here the measured data file representative of an S_{21} dip is used to extract f_r and the 3 dB bandwidth. This data is then used to compute Q_L using (2.7). Q_L is then used to compute Q_u using (2.8). Finally, the total attenuation is computed by (2.9) using the extracted f_r , computed Q_u , and the accurate determination of ϵ_e .

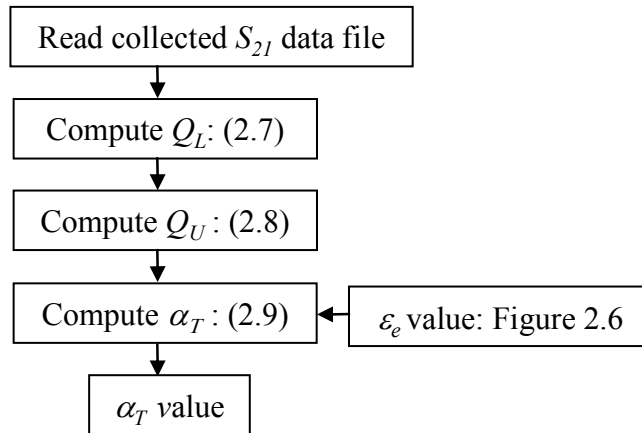


Figure 2.7 Total attenuation calculation flowchart

2.3 Dielectric and conductor property extraction

The total attenuation can be found for microstrip stubs of approximately equal length but different characteristic impedance. The total attenuation is

$$\alpha_T = \alpha_c + \alpha_d + \alpha_r \quad (2.10)$$

where α_c , α_d and α_r are conductor, dielectric and radiation attenuation, respectively.

The conductor attenuation is a function of metal conductivity as well as surface roughness at the metal-dielectric interface, lumped together in the term sheet resistance, R_s . We use the relationship between R_s and α_c developed by Pucel *et al* [17]:

$$\begin{aligned} \text{For } 0 < \frac{w}{h} \leq \frac{1}{2\pi}, \quad \alpha_c (dB/m) &= \frac{8.686R_s}{Z_0h} b_1 b_2 \\ \text{For } \frac{1}{2\pi} \leq \frac{w}{h} \leq 2, \quad \alpha_c (dB/m) &= \frac{8.686R_s}{Z_0h} b_1 b_3 \\ \text{For } \frac{w}{h} \geq 2, \quad \alpha_c (dB/m) &= \frac{8.686R_s}{Z_0h} b_3 b_4 b_5^2 \end{aligned} \quad (2.11)$$

where

$$b_1 = \frac{1}{2\pi} \left[1 - \left(\frac{w_e}{4h} \right)^2 \right]$$

$$b_2 = 1 + \frac{h}{w_e} + \frac{h}{\pi w_e} \left(\ln \left(\frac{4\pi w}{t} \right) + \frac{t}{w} \right)$$

$$b_3 = 1 + \frac{h}{w_e} + \frac{h}{\pi w_e} \left(\ln \left(\frac{2h}{t} \right) - \frac{t}{w} \right)$$

$$b_4 = \frac{w_e}{h} + \frac{\frac{w_e}{\pi h}}{\frac{w_e}{2h} + 0.94}$$

$$b_3 = \frac{w_e}{h} + \frac{2}{\pi} \ln \left(2\pi e \left(\frac{w_e}{2h} + 0.94 \right) \right)$$

In the equation for b_3 , e is the natural log base (2.718). The effective width, w_e , corrects width to account for metal thickness [18]:

$$\begin{aligned} w_e &= w + \frac{1.25t}{\pi} \left[1 + \ln \left(\frac{4\pi w}{t} \right) \right] \text{ for } \frac{w}{h} \leq \frac{1}{2\pi}, \\ w_e &= w + \frac{1.25t}{\pi} \left[1 + \ln \left(\frac{2h}{t} \right) \right] \text{ for } \frac{w}{h} \geq \frac{1}{2\pi}. \end{aligned} \quad (2.12)$$

Finally, Z_0 is the characteristic impedance of the microstrip line accounting for metal thickness [19]:

$$\begin{aligned} Z_0 &= \frac{60}{\sqrt{\epsilon_e}} \ln \left[\frac{8h}{w_e} + 0.25 \frac{w_e}{h} \right] \text{ for } \frac{w}{h} \leq 1, \\ Z_0 &= \frac{120\pi}{\sqrt{\epsilon_e}} \left[\frac{w_e}{h} + 1.393 + 0.667 \ln \left(\frac{w_e}{h} + 1.444 \right) \right]^{-1} \text{ for } \frac{w}{h} \geq 1. \end{aligned} \quad (2.13)$$

The dielectric attenuation is a function of loss tangent, $\tan \delta$, related by the expression [20]

$$\alpha_d (dB/m) = \frac{8.686 k_0 \epsilon_r (\epsilon_e - 1) \tan \delta}{2\sqrt{\epsilon_e} (\epsilon_r - 1)}. \quad (2.14)$$

Here, k_0 is the free space phase constant,

$$k_0 = \frac{2\pi}{\lambda_0} = \frac{2\pi f}{c}.$$

The attenuation resulting from power radiated from an open-ended quarter wave resonant stub is adapted from [11]:

$$\alpha_r (dB/m) = \frac{8.686 \left(480\pi h^2 R f_r^3 \sqrt{\epsilon_e} \right)}{Z_0 c^3}, \quad (2.15)$$

where

$$R = \frac{\epsilon_e + 1}{\epsilon_e} - \frac{[\epsilon_e - 1]^2}{2\epsilon_e^{3/2}} \ln \left[\frac{\sqrt{\epsilon_e} + 1}{\sqrt{\epsilon_e} - 1} \right].$$

This expression matches experimental results by Denlinger who asserts that no more than 25% of the total attenuation will be attributed to radiation loss for a microstrip transmission line resonator if $h/\lambda < 0.01$ and $\epsilon_r > 2.5$ [12]. The values obtained for radiation loss in our efforts were significantly less than the stated maximum 25%, usually below 0.01%, and met the above conditions as $h/\lambda = 0.002$ and $\epsilon_r = 9.5$.

Since α_T is known for two lines, the two properties R_S and $\tan\delta$ can be extracted. This is done by plotting a line of all possible combinations of R_S and $\tan\delta$ corresponding to the α_T for each stub, and then locating the point of intersection for the resultant pair of plots. Figure 2.8 outlines the approach for the extraction of loss tangent and sheet resistance. First, the attenuation due to radiation, α_r , is computed using (2.15). Then, a compensated value of total attenuation, $\alpha_{T\text{Compensated}}$, is calculated by subtracting α_r from α_T . A value of sheet resistance, $R_{S\text{Max}}$, that assumes all radiation compensated attenuation comes from α_c is calculated using $\alpha_c = \alpha_{T\text{Compensated}}$ in (2.11). A vector, R_S vector, is then formed for values from 0 to $R_{S\text{Max}}$. This vector is then used to compute a vector for α_c , α_c vector, by entering values computed in the R_S vector into (2.11). A vector for α_d , α_d vector, is computed by subtracting each value of the α_c vector from $\alpha_{T\text{Compensated}}$. Then a $\tan\delta$ vector is formed by entering each value of the α_d vector and accurate ϵ_e value into

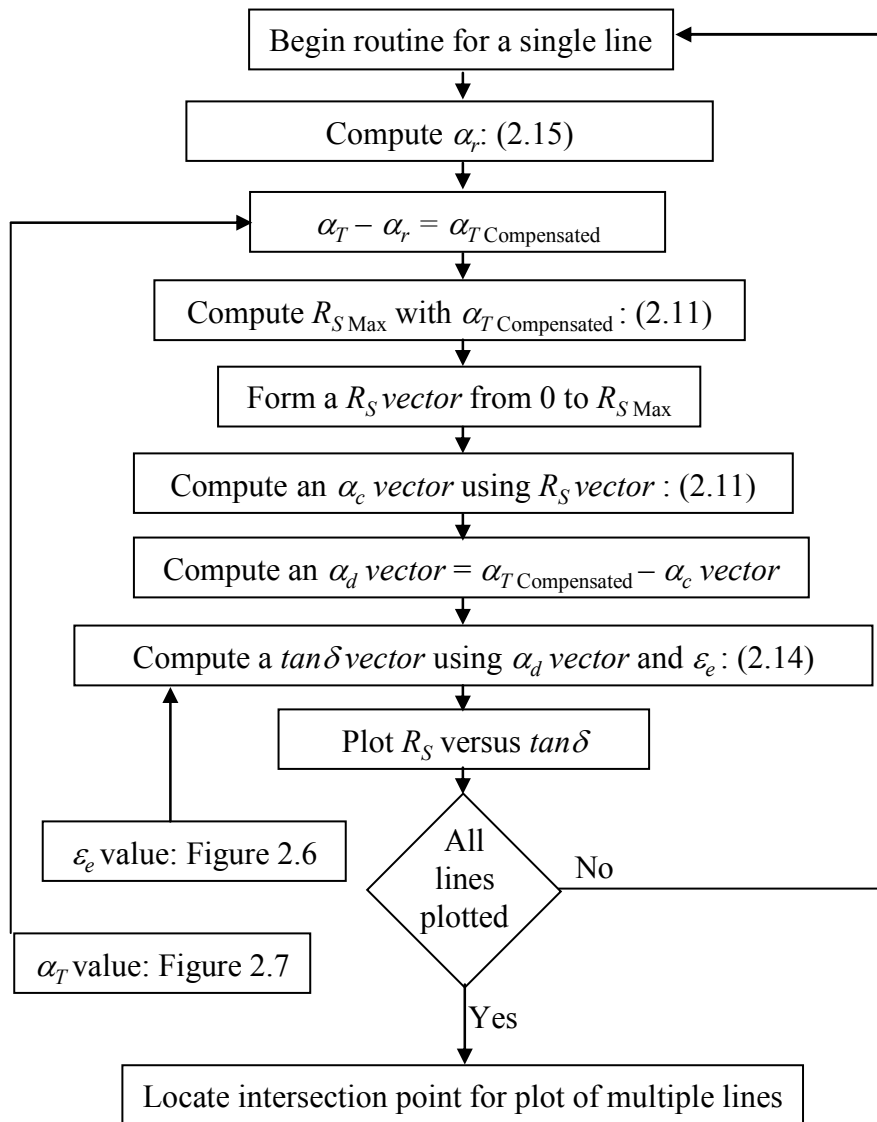


Figure 2.8 Extraction of R_S and $\tan\delta$ flowchart

(2.14). Finally, the R_S vector and the $\tan\delta$ vector are used to plot the line representative of all possible combinations of R_S and $\tan\delta$ for a single resonator stub operating at a specific resonance mode, N. This entire process is repeated for the second stub resulting in two lines of differing slopes. The intersection point of these two lines indicates the

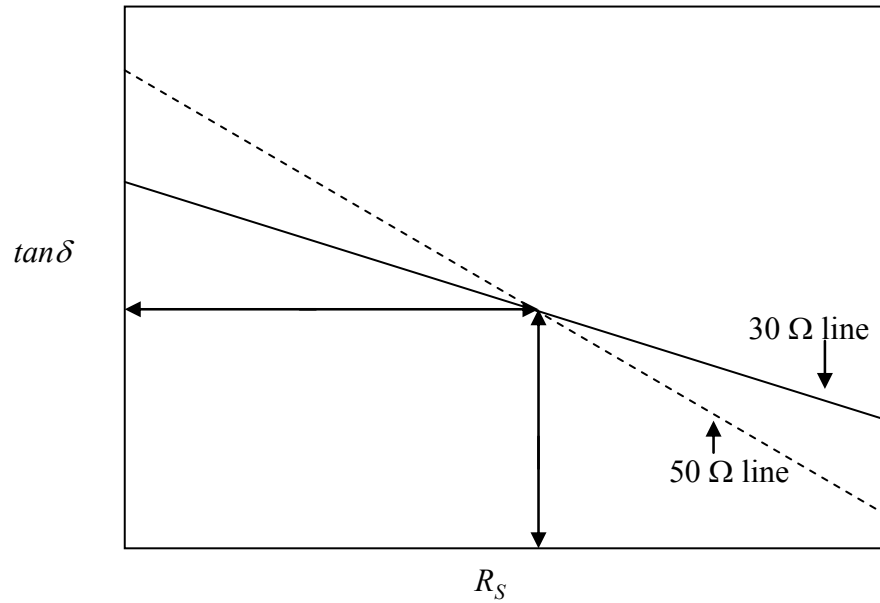


Figure 2.9 Ideal intersection plot for a pair of tee resonators that shows how $\tan\delta$ and R_S are extracted

value of R_S and $\tan\delta$. Figure 2.9 serves as a demonstration of the type of plot generated by the aforementioned methodology.

CHAPTER 3
BOARD PREPARATION

3.1 Fabrication

Test boards in the microstrip configuration were developed using a ceramic substrate as the dielectric and a conductive paste as the conductor. Materials and the associated data sheets needed to construct these test boards were then obtained from the manufacturers. Alumina (96% alumina, 4.5 inches square, 25 mils thick, from Coors Ceramic, Co.) was used as the substrate material. Silver/Palladium conductive paste (6/1 Ag/Pd from Heraeus) was used to form the conductors. The modeling software suite used in the design of the tee resonator test vehicle was the very efficient and powerful Agilent Advanced Design System (ADS). This was done with the intention to use the board space as efficiently as possible. The design consisted of four resonators and a

Table 3.1 Tee resonator and calibration line design dimensions

	f_r (GHz), (N=1)	line length L (mil)	line width w (mil)
calibration line *		3000	24.87
through line **		3000	24.87
50 Ω stub	0.8	1460.98	24.86
30 Ω stub	0.8	1396.25	60.88
50 Ω stub	2.4	485.55	24.84
30 Ω stub	2.4	463.29	60.83
<i>* line used for calibration (see Figure 3.1)</i>			
<i>** each resonator stub has a through line attached to it (see Figure 3.1)</i>			

calibration line. The design parameters of the resonators were a first resonance (N=1) of 800 MHz for the two longer resonators, and a first resonance (N=1) of 2.4 GHz for the two shorter resonators. The resultant dimensions representative of the design of the four resonators and the calibration line are shown in Table 3.1.

The resonances are chosen so that the 2nd (N=2) resonance of the longer resonators would match the 1st (N=1) resonance of the shorter resonators as a further attempt to confirm results. Both the long set and short set of resonators were chosen to have resonator stubs of differing characteristic impedances. This effectively provided one long stub and one short stub at 50 Ω and one long and one short stub at 30 Ω . The physical parameters, width and length, of each resonator and the through line were then

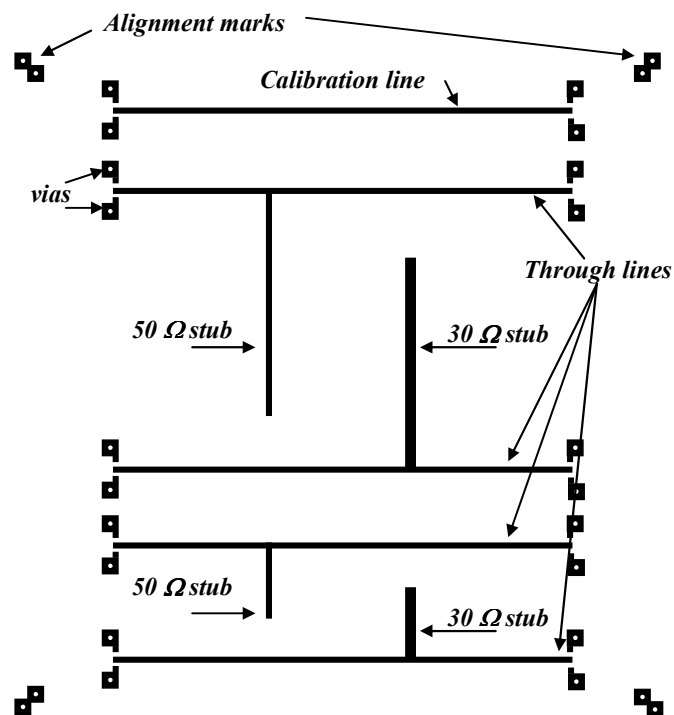


Figure 3.1 Lavenir layout for tee resonators and calibration line

recorded. This data was then used to create the board layout using Lavenir CAD software. The resultant layout created using this software is shown in Figure 3.1. It is important to note that there are actually two layouts created. The layout shown is for the resonators and thru line on the top of the alumina substrate. The other layout created is a single black square representative of the groundplane covering the bottom of the substrate. This layout is not shown due to its self explanatory nature.

A gerber file representative of the layout shown in Figure 3.1 was created to be

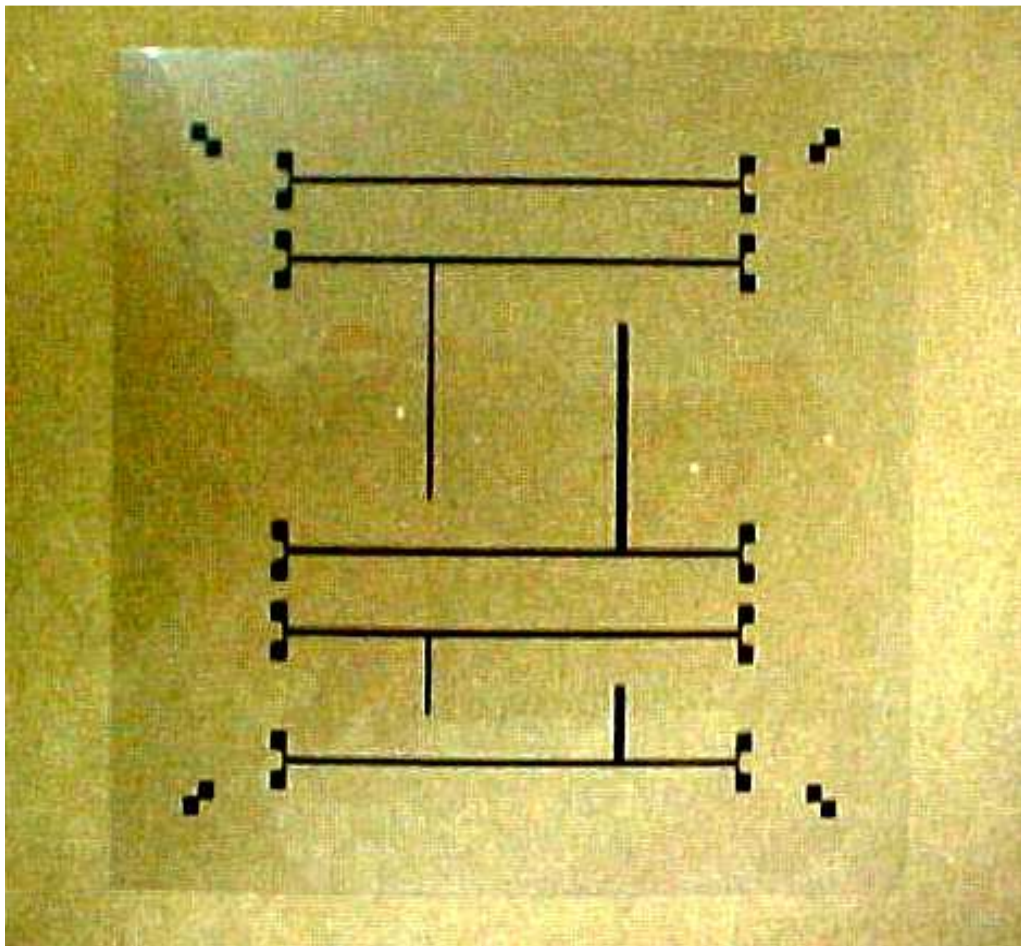


Figure 3.2 Mask for tee resonators and calibration through line

used in the photoplotting process. The mask for the resonators and calibration line is shown in Figure 3.2. The masks were then used to expose photo-sensitive screens.

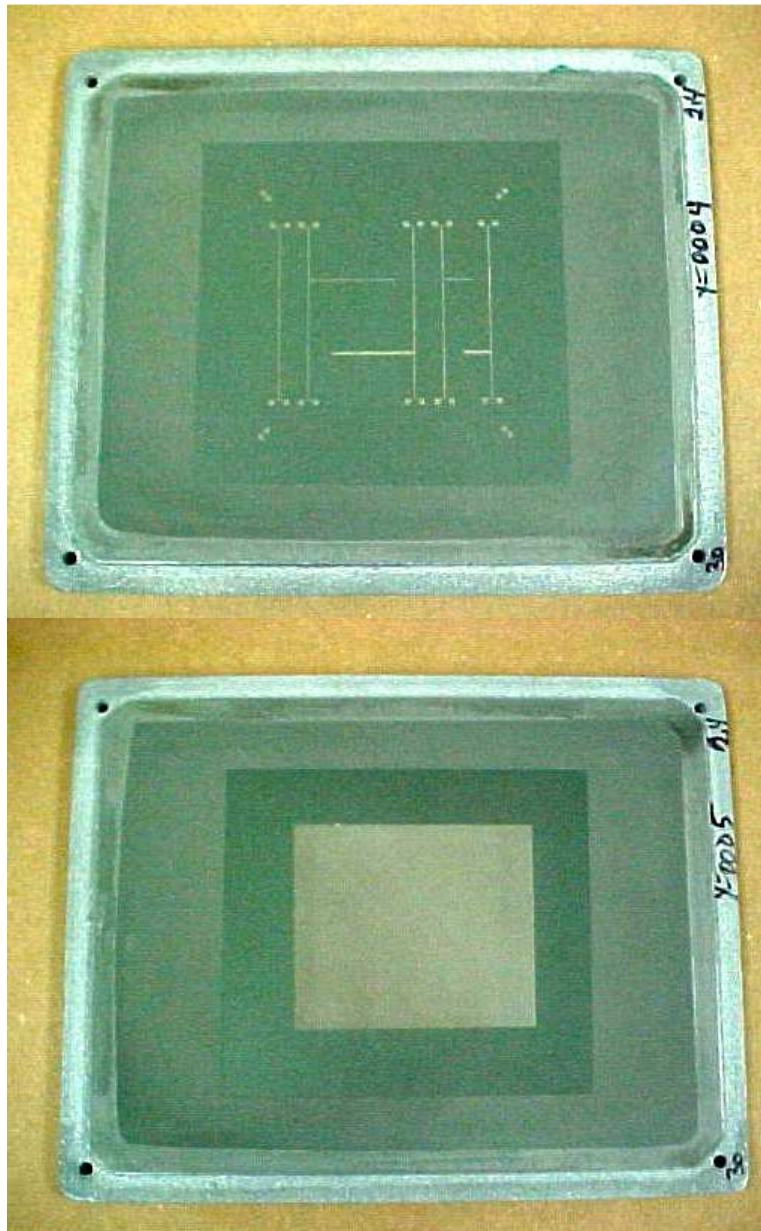


Figure 3.3 Screens for the resonators and groundplane

This process is performed by placing the mask over the area of the screen covered with photo-resist. The areas that are not covered by the mask are exposed to intense ultraviolet light. This causes the area exposed to solidify and become a permanent structure in the mesh of the screen. The areas that are covered are not solidified and are removed by a stream of water. These screens for both the tee resonator structures and the groundplane are shown in Figure 3.3. Once the screens are dry they can be used in the screenprinter shown in Figure 3.4. The appropriate settings are used to ensure that the proper amount of conductive paste is applied through the open sections of the mesh and onto the alumina substrate. The paste is first applied to the resonator side of the alumina substrate. After the paste is applied to the substrate it is immediately placed in



Figure 3.4 Screenprinter



Figure 3.5 Drying oven

the drying oven shown in Figure 3.5. The substrate is then taken from the drying oven and placed in the firing oven shown in Figure 3.6 for 90 minutes at



Figure 3.6 Firing oven

a central zone set-point temperature of 900 degrees Celsius. The screen printing, drying oven and firing oven processes were repeated for the groundplane. The boards were then drilled at high rpm using a diamond tip drill bit in the areas defined as vias in Figure 3.1. These holes were then filled with the Silver/Palladium conductive paste using a syringe.

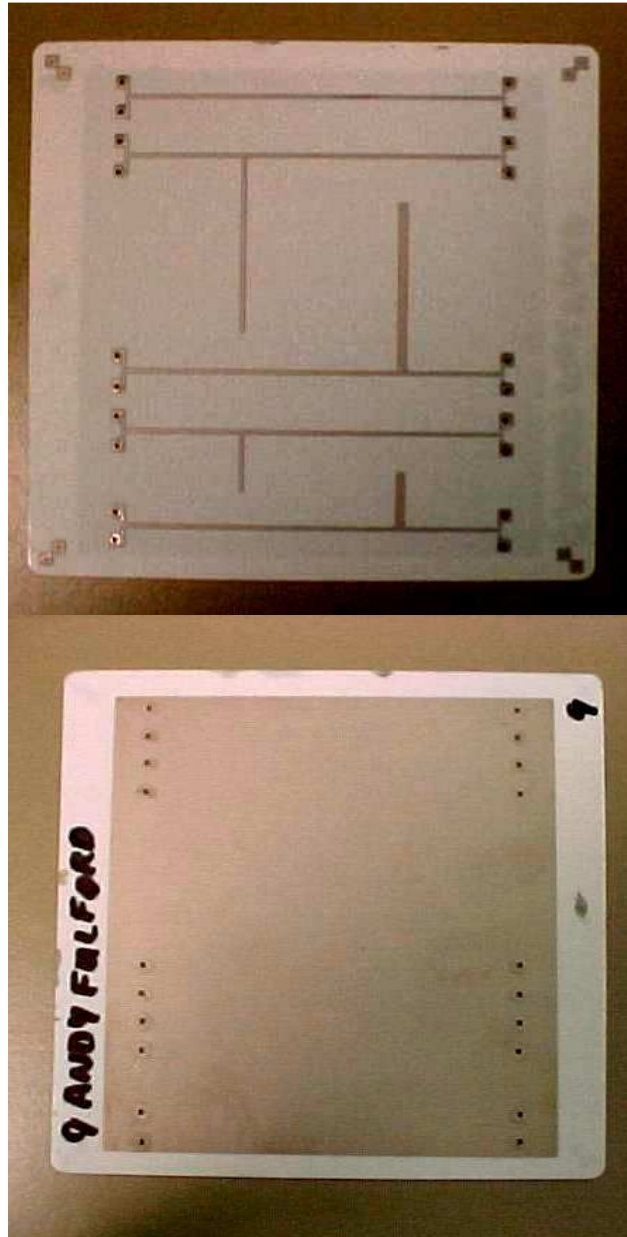


Figure 3.7 Completed microstrip tee resonator test structure

The boards were then cured in the firing oven at the above stated conditions. The filling procedure allowed a uniform coating along the interior of the via holes. This uniform coating allows a conductive path through the substrate from the via pad to the ground plane surface. The final result is a complete microstrip tee resonator test structure as shown in Figure 3.7.

CHAPTER 4

MEASUREMENTS

4.1 Measurement procedure

The transmission scattering parameter S_{21} , which corresponds to the amount of power transmitted through a two-port network, is measured using a Hewlett-Packard 8510C Vector Network Analyzer in conjunction with an Alessi Probe Station fitted with GGB Picoprobe 40A-GSG-1250-LP-HT probes. A probe contacting the board during measurement is shown in Figure 4.1. The complete test equipment setup is shown in Figure 4.2.

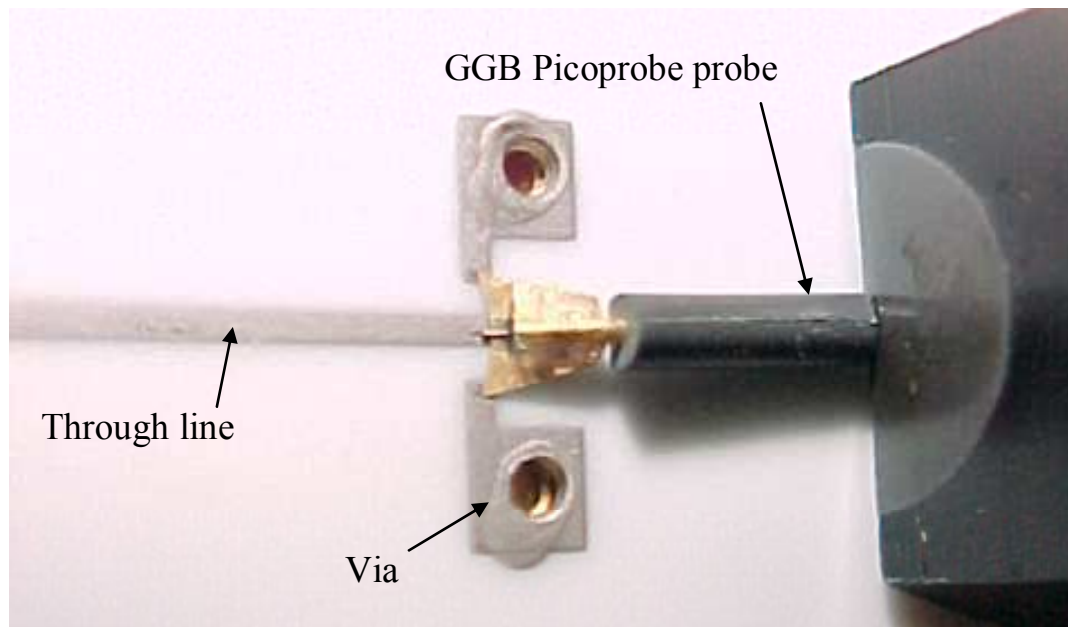


Figure 4.1 Probe in contact with board during testing

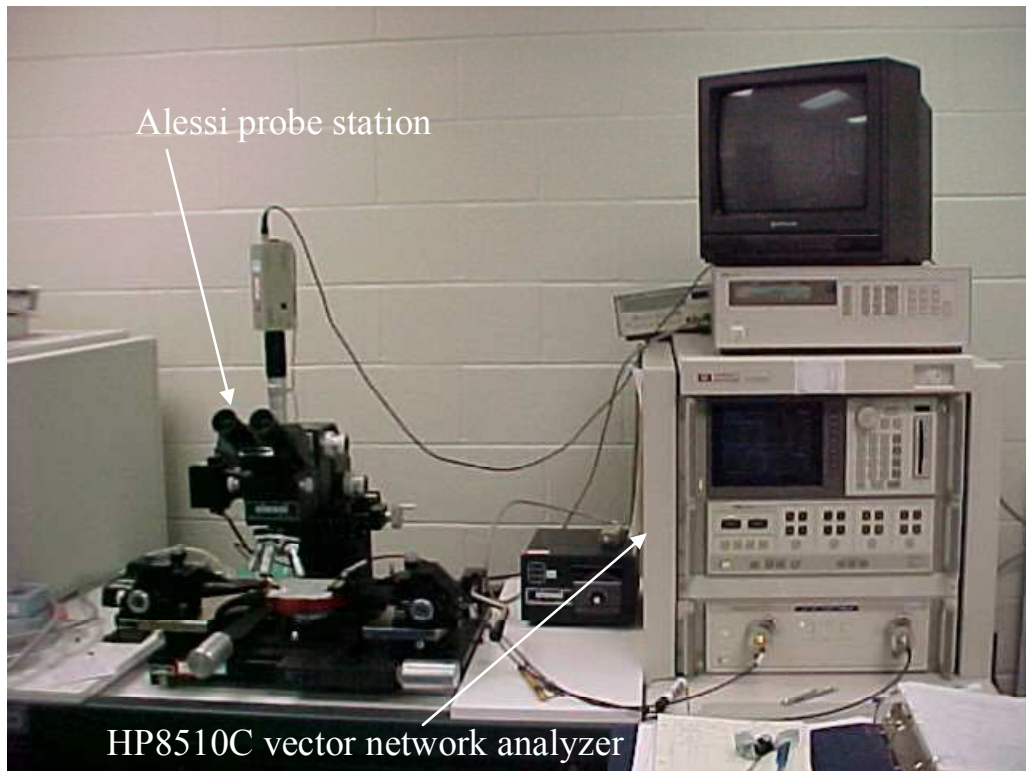


Figure 4.2 Testing equipment

The general approach to the data collection process involves taking an initial wideband measurement to locate the resonant frequencies, and then narrow band measurements are made to get sufficient accuracy in order to extract total attenuation. The measurements are performed with averaging on (32 points), smoothing off, and data output set to 201 points. The test vehicle in position for measurement on the Alessi probe station is shown in Figure 4.3.

4.1.1 Standard procedure

A standard procedure for performing network analyzer measurements was developed to ensure the accuracy of data collected. One procedure used to provide

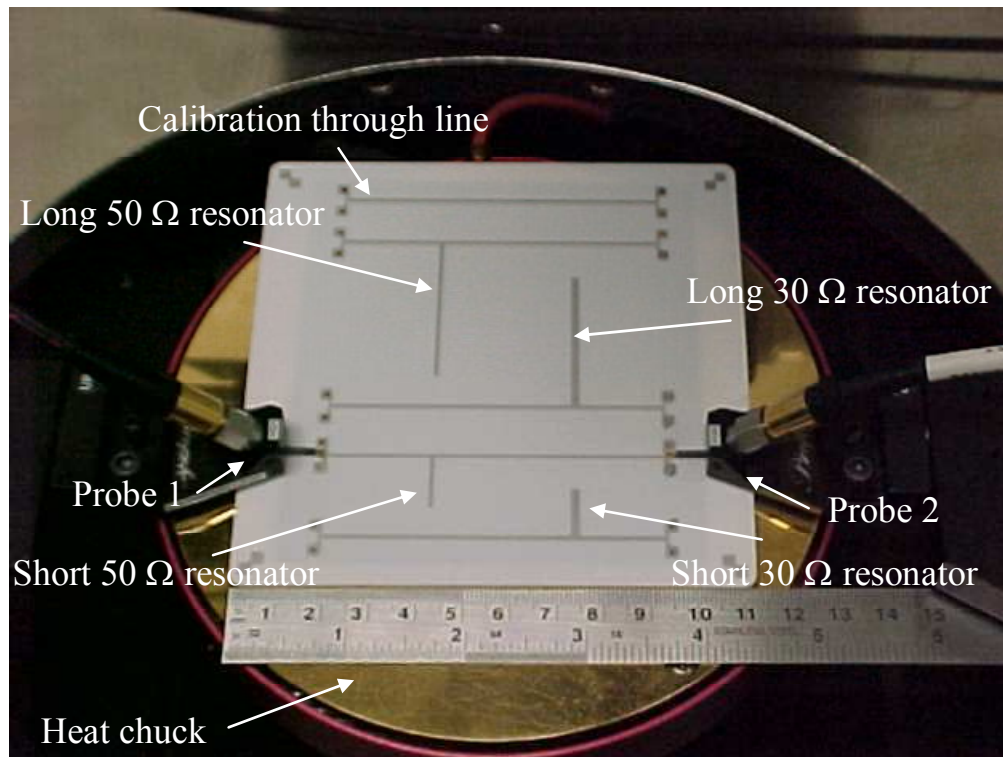


Figure 4.3 Test board during measurement on the Alessi probe station

assurance in the accuracy of data collected is a “through-response” calibration. This calibration is performed on the through line prior to the measurement of the resonators. Performing a calibration before resonator measurements allows the effects of the through line to be minimized or taken out of the tee resonator measurement. This allows a collection of data that is more representative of the resonator stub itself. It is important to note at this point that even though the through line for the resonators and the calibration line are of identical design, the small fabrication variances do not allow a 100% removal of the effects of the through line from the resonator measurement.

In addition, measures must be taken to ensure that the probes are adequately situated on the contacts. This is done in an effort to minimize measurement variance

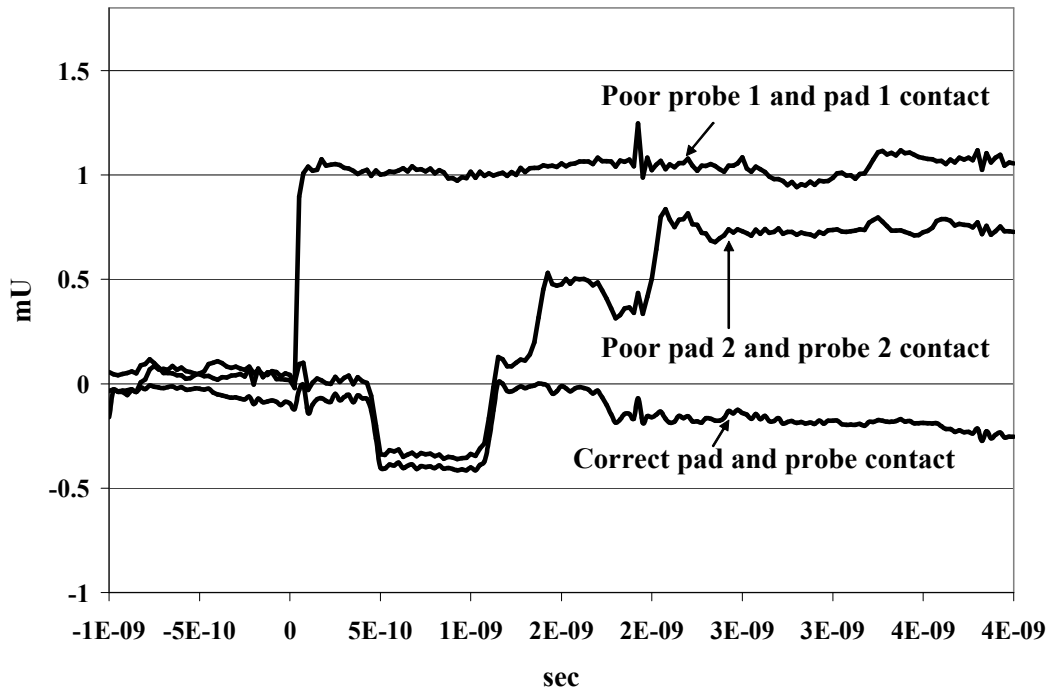


Figure 4.4 TDR signatures of correct and incorrect probe placement

induced by human error when making repeated probe contacts with the test pads. To minimize error in this step, we have employed time domain reflectometry (TDR) to assure a good contact between probe and pad. This step effectively produces a visible fully error-corrected transmission response of the structure in near real time [21]. TDR signatures for the cases of both good and poor probe and pad contacts are shown in Figure 4.4. Total attenuation was calculated using data from 30 repeated measurements on a single board with and without using TDR to determine the validity of this step in the measurement process. Note that this data was collected using the long 50 ohm resonator ($N=1 \Rightarrow \sim 800$ MHz). The results of this procedure can be viewed in Table 4.1. The standard deviation for the results using data collected with TDR was found to be 2 orders

Table 4.1 Average value and standard deviation of total attenuation with and without using TDR to place the probes

	Without TDR	With TDR
Number of Samples	30	30
Average Value	0.148	0.155
Standard Deviation	0.0022	0.000087

of magnitude less than the results not using TDR. This study confirmed the use of TDR as an important step in the measurement process.

The standard procedure for taking a measurement consists of five different steps. First, the connection of the probes and the vehicle calibration through line is validated using time domain reflectometry (TDR). Second, the calibration is set by performing a “through-response” calibration using the through line. Third, the probes are moved to the resonator where TDR is once again used to validate the proper connection between the probes and the resonator through line. Fourth, the calibration setting is enabled so that the proper dip is visible. An example of this would be the single dip at $N=1$ for the $50\ \Omega$ long resonator. Last, the data is stored on a floppy disc so that the data can be later transferred to a PC for processing.

4.1.2 *Variability study*

A measurement procedure variability study was performed to quantify expected error margins with the collected data. This study was performed for repeated measurements on a single board and measurements on multiple boards. This provided both same board and board-to-board variability. These measurements were performed at

Table 4.2 Measurement variability

Test Procedure	variability (+/-)**
Board #1 (15 samples, same board) @ room temp	0.6%
Board #2 (15 samples, same board) @ room temp	0.2%
Board #3 (15 samples, same board) @ room temp	0.4%
Average same board variability @ room temp	0.4%
Board #1 (5 samples, same board) @ 100 deg C	0.1%
Board to Board (8 different boards) @ 100 deg C	2.0%
Board to Board (11 different boards) @ room temp	2.0%
<i>**computed as the variability of the average S_{21} dip calculated over a 200 MHz bandwidth centered at the fundamental resonance frequency</i>	

room temperature and at 100 degrees Celsius. The results for both repeated single board measurement variability and board-to-board measurement variability are listed Table 4.2.

The repeated measurements on a single board were done in an effort to quantify the variability of the current testing procedure for a single test vehicle. This repeated measurement testing process consisted of 15 measurements on three different test vehicles at room temperature. The same process was performed for 5 measurements on board 1 at 100 degrees Celsius in order to quantify the effect of elevated temperature on measurement variability. Each of these measurements was taken using the standard five step measurement taking procedure outlined in the previous sub-section. The long 50 Ω resonator, operating at the resonance mode N=1 (785 MHz), was the test structure used. The average variability of plus or minus 0.4 percent at room temperature and 0.1 percent at 100 degrees Celsius shows that the testing procedure itself results in a promising total average variability of 0.8 percent at room temperature and 0.2 percent at 100 degrees Celsius.

Board-to-board variability was the next topic examined. Eleven different boards at room temperature and eight boards heated to 100 degrees Celsius were tested in order to measure the variability of measurements from board to board. Each test vehicle was examined using the standard five step measurement taking process. The 50-ohm long tee resonator operating at the first resonance was the structure used in this board-to-board testing. The average board-to-board variability was found to be plus or minus 2 percent. It was discovered that the variability for board-to-board measurements was higher than the variability for repeated measurements on the same board

4.2 Property extraction

The substrate permittivity, total attenuation, sheet resistance, and loss tangent can be calculated using MATLAB coding based on the approach discussed in Chapter 2. This coding is given in the appendix for further explanation. The physical dimensions of the test boards were measured in order to improve the accuracy of the extracted properties. The thickness of the conductive paste was measured using a profilometer as approximately 0.4 mils. The physical dimensions of the tee resonators on a finished test board were also measured using a microscope. This and all other data used in the property extractions are listed in Table 4.3.

4.2.1 *Permittivity extraction*

The effective and relative permittivity are computed using the typical physical parameters listed in Table 4.3 and the measured resonant frequency for a resonator operating at a specified resonance mode. The resonant frequency is the most negative

Table 4.3 Typical data for the test board

$Z_0 (\Omega)$	50	30
through line width (mil)	25	25
t (mil)	0.4	0.4
h (mil)	25	25
$\tan\delta$ (Coors data sheet)	4.0×10^{-4}	4.0×10^{-4}
short resonator pair		
w (mil)	25	61
L (mil)	486	463
long resonator pair		
w (mil)	25	61
L (mil)	1461	1396

point of a S_{21} dip collected using the standard measurement procedure. The typical extracted permittivity values for the long and short pairs of resonators operating at their respective first resonance modes are listed in Table 4.4. The ϵ_r for the long 50 Ω

Table 4.4 Typical permittivity extraction results

$Z_0 (\Omega)$	50	30
short resonator pair		
f_r (GHz)	2.37	2.44
ϵ_e	6.34	6.57
ϵ_r	9.44	8.92
long resonator pair		
f_r (GHz)	0.785	0.782
ϵ_e	6.55	7.21
ϵ_r	9.78	9.83

resonator was 9.78, while the long 30 Ω resonator had $\epsilon_r = 9.83$. These values are slightly higher than the ones on the data sheet provided by the substrate manufacturer (Coors Ceramics, $\epsilon_r = 9.5$). The short pair of resonators had a value of relative permittivity that was slightly lower than the manufacturer's stated value.

The variability of this extraction process was also examined using the extraction of relative permittivity. The testing of this process involved the plotting of relative permittivity for the long 50 ohm resonator versus the long 30 ohm resonator. This procedure was performed for the modes N=1 through N=3 on 8 separate test vehicles. The purpose of this type of plot, shown in Figure 4.5, was to quantify the amount of variability in the extraction of relative permittivity for the two different resonators. The

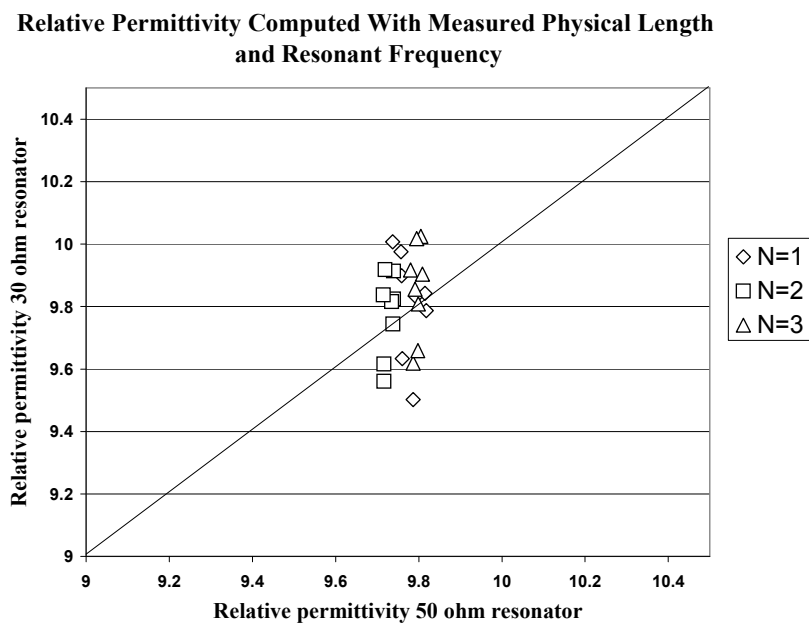


Figure 4.5 Plot of long 30 ohm resonator relative permittivity vs. long 50 ohm resonator relative permittivity

tighter grouping of the values in the horizontal direction suggests that the data for the 50 ohm resonator has less variability than that of the 30 ohm resonator.

4.2.2 Total attenuation extraction

Data points corresponding to a dip of the type shown in Figure 4.6 form the data file collected during measurement that is used to extract total attenuation. A MATLAB routine pulls resonant frequency, 3 dB bandwidth and S_{21R} from this file. This data and the previously computed effective permittivity are used to calculate a value of total attenuation. The typical results of this process are shown in Table 4.5.

Improvement in the attenuation extraction routine was realized. Attenuation is calculated by feeding the collected S_{21} data into a MATLAB program. The analyzer

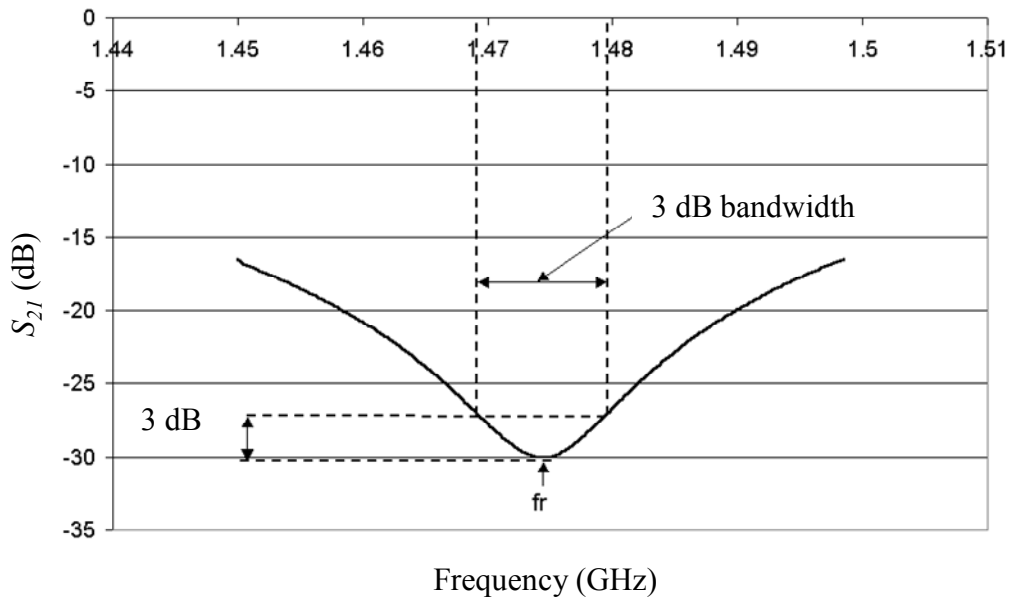


Figure 4.6 Single dip used for attenuation calculation

Table 4.5 Typical total attenuation extraction results

$Z_0(\Omega)$	50	30
short resonator pair		
f_r (GHz)	2.37	2.44
S_{21R} (dB)	-30	-37
BW_{3dB} (GHz)	0.046	0.035
Q_L	51.6	69.5
Q_U	51.7	69.5
α_T (dB/in)	0.267	0.208
long resonator pair		
f_r (GHz)	0.785	0.782
S_{21R} (dB)	-26	-31
BW_{3dB} (GHz)	0.026	0.025
Q_L	30.1	30.9
Q_U	30.2	30.9
α_T (dB/in)	0.155	0.158

allows selection of number of measurement data points. We selected 201 data points, (as opposed to 401 or 801) for most rapid measurement and data recording. However, this led to discretization error in the MATLAB routine as frequency bandwidth was determined. To get more accurate results, an interpolation routine was added to the attenuation extraction program. For each of 30 measurements, Figure 4.7 compares attenuation using the original MATLAB routine, without interpolation, to the more accurate approach using interpolation. We see that without interpolating, the MATLAB routine was rounding the data and losing some accuracy. The addition of interpolation

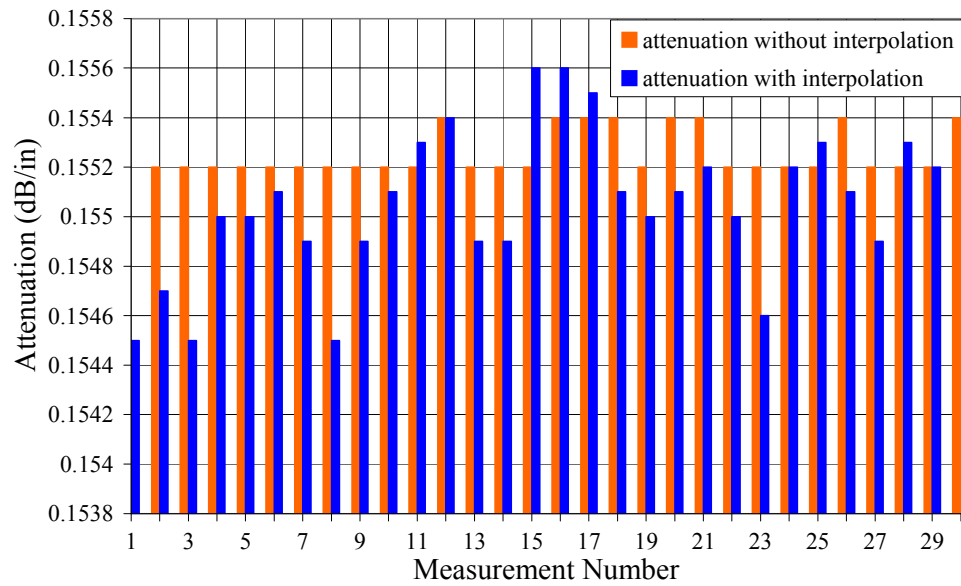


Figure 4.7 Chart comparison of 30-sample study of long 50 Ω tee resonator with (black) and without (grey) the MATLAB interpolation addition

improves the measurement accuracy, but by doing so it also results in more variability as shown in Table 4.6.

Table 4.6 Interpolation addition results

	with interpolation	without interpolation
Number of Samples	30	30
Average value (total attenuation (dB/in))	0.155	0.155
Standard Deviation	0.00029	0.000087

4.2.3 Sheet resistance and loss tangent extraction

For a given impedance stub, a combination of all possible values of $\tan\delta$ versus R_S that give the measured total attenuation can be plotted. The resulting line will have a distinctive slope for each impedance stub. A typical R_S versus $\tan\delta$ plot is shown in Figure 4.8. Here, the intersection of the lines for the 30 Ω and 50 Ω stubs gives $\tan\delta = 13 \times 10^{-4}$ and $R_S = 67$ milliohms per square. Assuming a very smooth copper line of the same thickness as our lines, a simple best-case estimate of R_S would be 14 milliohms per square. This value is calculated as [3]:

$$R_S = \sqrt{\frac{2\pi f_r \mu}{2\sigma}} \quad (4.1)$$

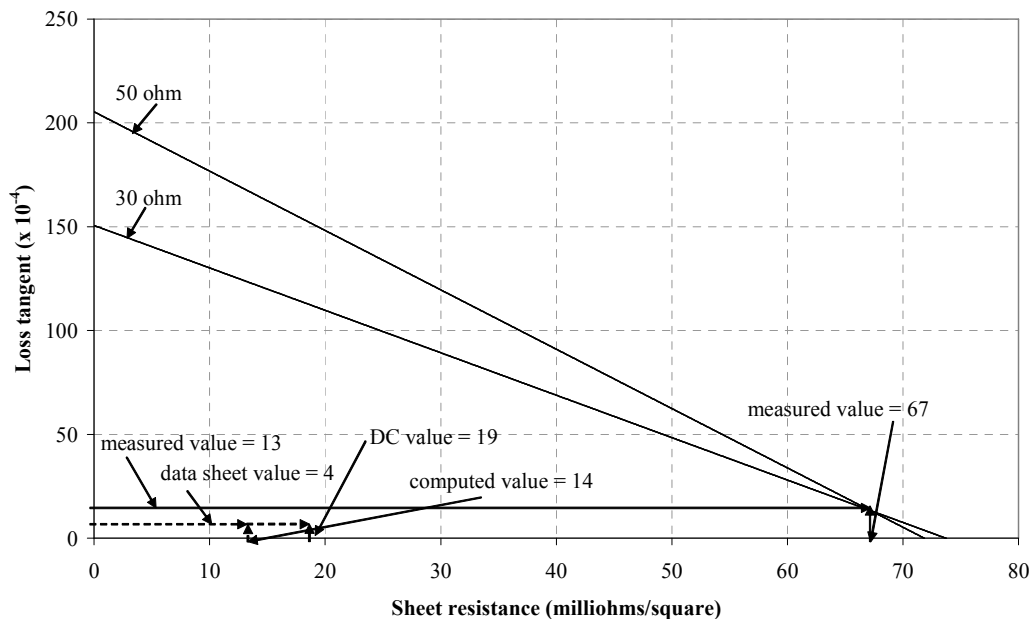


Figure 4.8 Plot of sheet resistance vs. loss tangent using measurements on a 30 Ω and 50 Ω tee resonator pair

For comparison, a DC sheet resistance value of 19 milliohms per square was measured on the calibration line of the test board. Our extracted value, using less conductive Ag/Pd paste on a substrate that is not perfectly smooth has a significantly higher R_S than this. Finally, the substrate data sheet indicated a loss tangent, at 1 MHz, of about 0.0004. Our value is slightly over three times this value.

CHAPTER 5

SIMULATION

Simulation using available software suites was used to further examine the accurateness of the extracted values obtained using data from measurements on the test board. These software suites were used to both validate the design of the test board and to examine the extraction routine itself. This allowed the confirmation of the operation of the resonators on the test board and the performance of the extraction routine void of physical constraints such as measurement variability and possible flaws in the finished test board.

5.1 Board design verification

Tee resonators can be designed with current computer aided design (CAD) simulation software to meet the established particular electrical design parameters within the limits of physical fabrication tolerances [15,22-29]. For this reason, modeling software suites were employed in the design of the resonator structure. This allowed the microstrip tee resonator test vehicle to be effectively tested to ensure proper operation before the time consuming fabrication processes were undertaken.

The modeling software suite used in the design of the tee resonator test vehicle was ADS. This software package allows a very wide range of options with regards to the

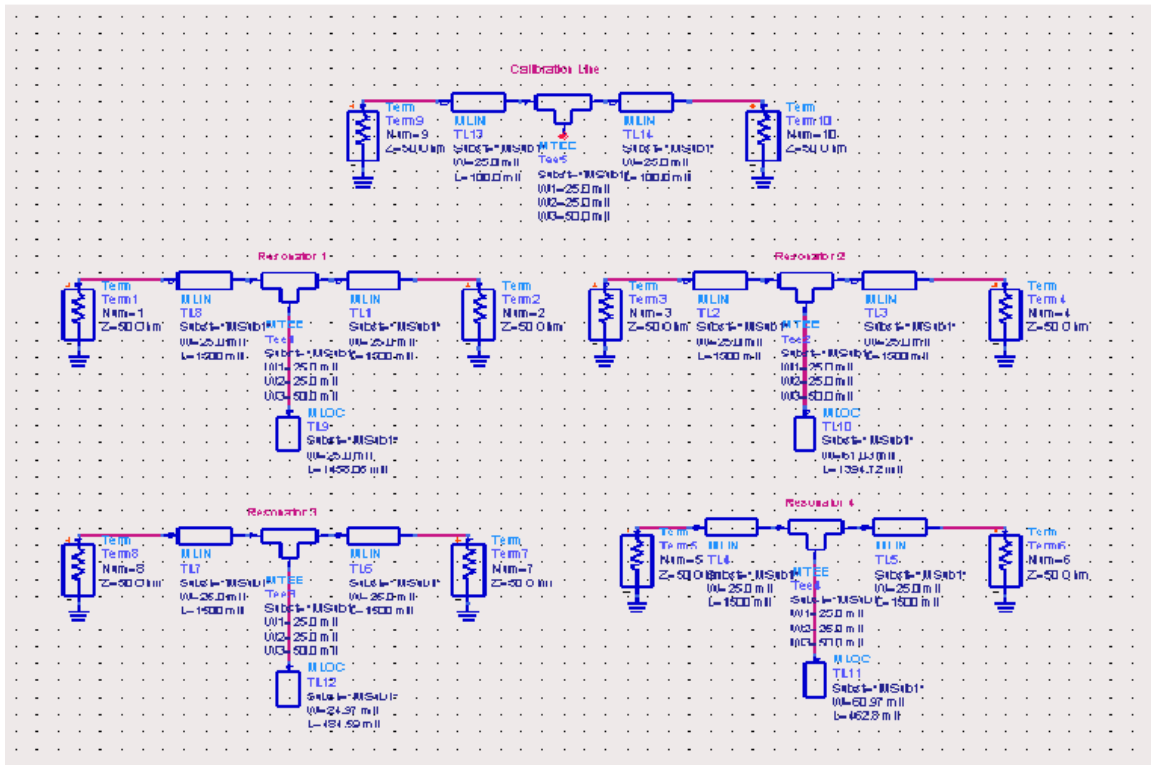


Figure 5.1 ADS schematic layout used in the design of the test board

actual computation method used. “Schematics” is a symbolic environment that allows the placement of representative parts from libraries to form the structure of interest. This environment has both its advantages and disadvantages. The environment allows a user with limited experience to accurately design circuits for simulation. This type of software also allows the user to employ tools that generate quick design parameters and results for a model. A significant disadvantage of this design environment is that it relies upon quasi-static approximations for the computation of results [24-28]. The final design of the four resonators and the calibration through line can be viewed in Figure 5.1. The use of this software also allowed a simulation to be performed for each resonator to

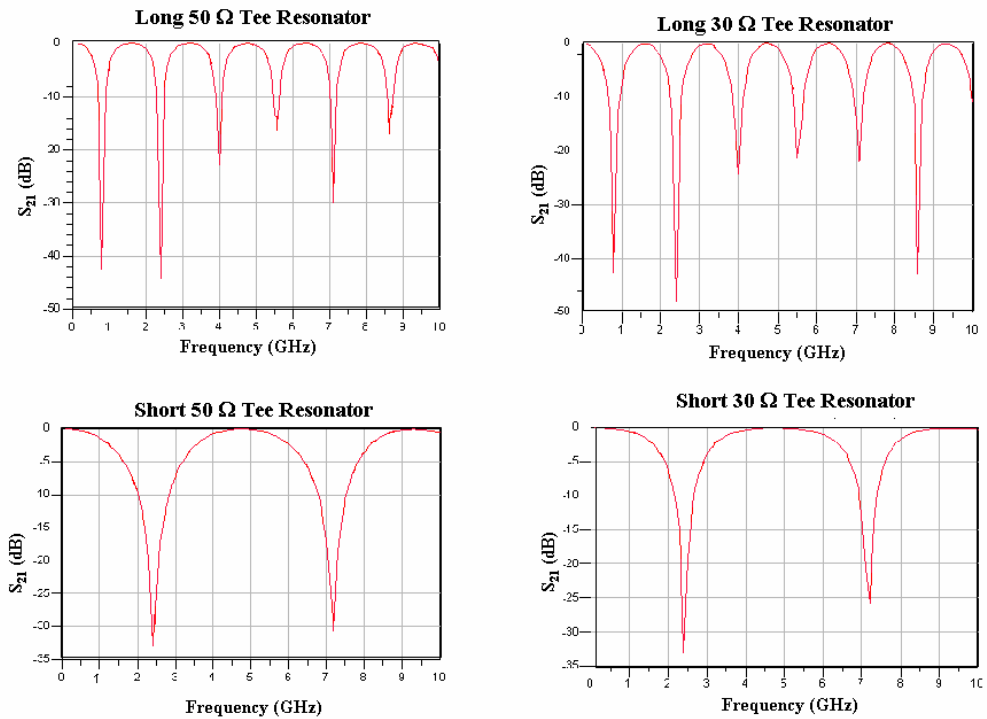


Figure 5.2 Resonant dips used for confirmation of the design of the four resonators

confirm that the resonant dips occurred at the correct locations. These resonant dips generated by ADS are shown in Figure 5.2.

5.2 Modeling Approach

The modeling of the microstrip tee resonator structure was also performed in an effort to examine the property extraction process discussed in Chapter 2. Performing simulations for models of the tee resonator designed to match the design criteria of the test board allows a generation of data that is similar to the data collected by measurements. This S_{21} data in the form of the characteristic dip can be generated with the parameters known. This gives an advantage over the data collected using the test

board in that the model parameters can be directly compared with the results computed using the extraction routine. It is important to note that the accuracy of the generated data relies heavily on the model design itself [15,22-29]. This modeling process was performed using two different software suites.

5.2.1 ADS “momentum”

“Momentum” is the environment in ADS that was used to study the property extraction procedure discussed in Chapter 2. Momentum is very versatile in that it allows several different types of simulation sweep schemes and meshing strategies. “Momentum” operates on the principle of finite element modeling (FEM). This type of numerical computation is stated as being less accurate at replicating the behavior of an exact physical model when compared to other modeling schemes [22,23]. This, however, is compensated for by the fact that ADS uses techniques such as adaptive sweep and single layer approximation to give very accurate results with a significantly lower amount of required computing power.

5.2.2 Flomerics micro-stripes

Flomerics micro-stripes is another powerful modeling suite used in the examination of the property extraction process. Micro-stripes is a software package developed to simulate electromagnetic phenomena in a consistent and reliable manner [22,23]. This is accomplished by using the Transmission Line Modeling (TLM) method of numerical analysis. The use of this method of computation is very accurate in modeling structures and cavities at microwave frequencies [22]. This is currently the

only computational method that allows a user to create a physical model with an exact solution [22,23]. The TLM method is a three-dimensional modeling scheme that involves the computation of both shunt and series elements resulting in a true three-dimensional representation of the model [23]. The application of this theory in the use of the micro-stripes software package has both advantages and disadvantages. The advantage is that it uses the TLM method described above and thus can give very accurate results when compared to physical models. The disadvantage is that this type of computation requires very tightly meshed models to give these highly accurate results. The tightly meshed model requires the number of cells to range on the order of millions to achieve highly accurate results. The time required to compute results for each model is dependant upon both the total number of cells and the physical size of the cells. This is a significant factor due to the time required to perform each successive simulation.

5.2.3 *Property extraction verification approach*

The use of these software packages in the examination of the property extraction process involves an iterative approach shown in Figure 5.3. First, the values that define the behavior of the model are decided and recorded for later use. These values include parameters such as relative permittivity and loss tangent for the dielectric, the conductivity of the metal used for the conductors, and the physical dimensions of the components that define the complete microstrip test structure. Then, the model is designed using these values. The model is then simulated at the decided conditions. These conditions include the meshing resolution, frequency span, and type of simulation sweep plan. The meshing resolution is the number of cells per wavelength used in the

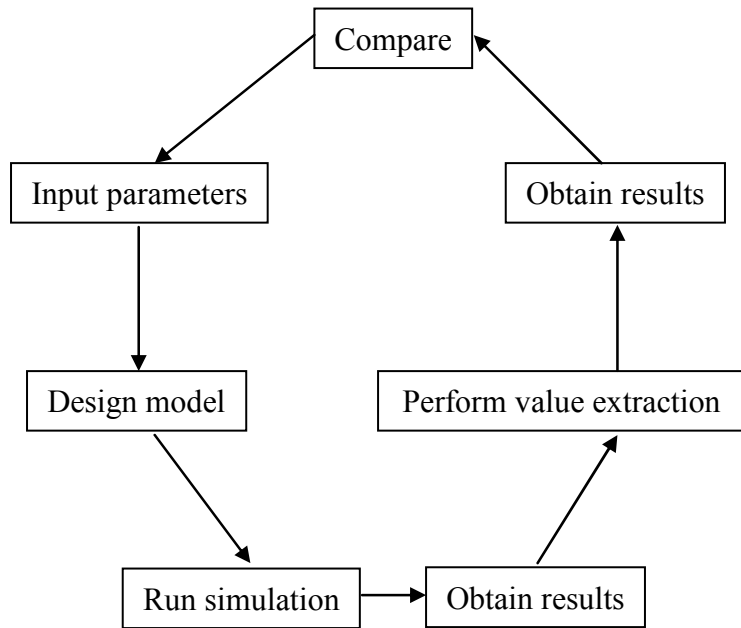


Figure 5.3 Property extraction verification approach using modeling

model design. The frequency span is the start and end point in frequency that the simulation is performed. The type of simulation sweep span is either adaptive or linear. In our experience it was found that the adaptive sweep plan in ADS is used for results that are quick but less precise. The linear sweep plan takes much more time to complete but it also provides the necessary accuracy. The results of interest are in the form of a single S_{21} dip. This single dip provides the resonant frequency and 3dB bandwidth information for the model of the tee resonator that was simulated. Then the properties are extracted using MATLAB coding that was developed based on the process described in Chapter 2. The results from this coding routine are then compared to the values used in the design of the model that was simulated. This process is repeated for a number of

different resonators at different conditions. This is done in an effort to understand the behavior of the property extraction procedure defined in Chapter 2.

5.3 Results

5.3.1 Model meshing resolution

Meshing resolution or the number of cells per wavelength contained in the structure of interest was found to have a great influence on the generated data. The resonant frequency generated for a single resonator modeled using micro-stripes was observed in an effort to understand the influence of model meshing resolution. Several simulations for this model were performed. In each simulation, the size of the cells was decreased resulting in an increase in the resolution of the model's meshing. The

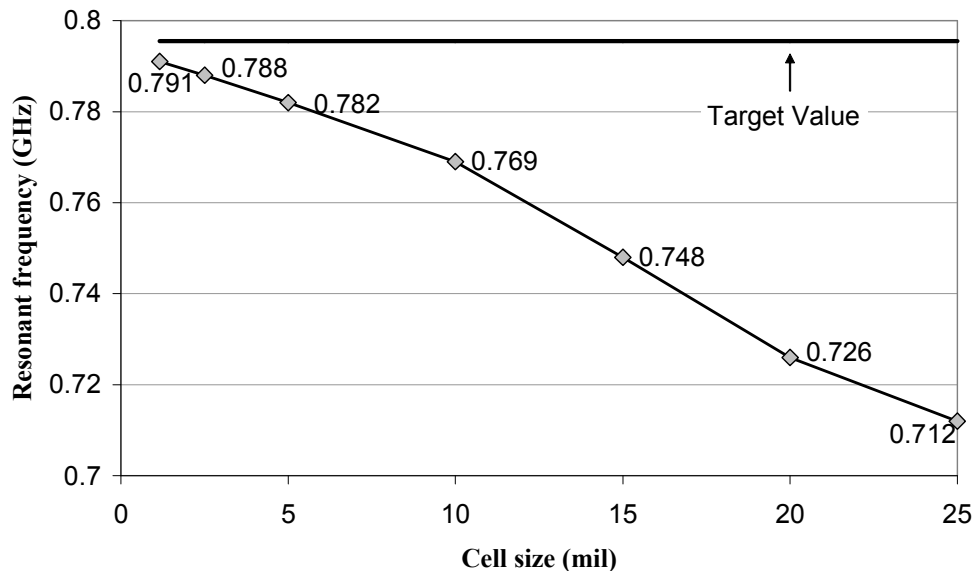


Figure 5.4 Progression of resonant frequency towards target value using micro-stripes

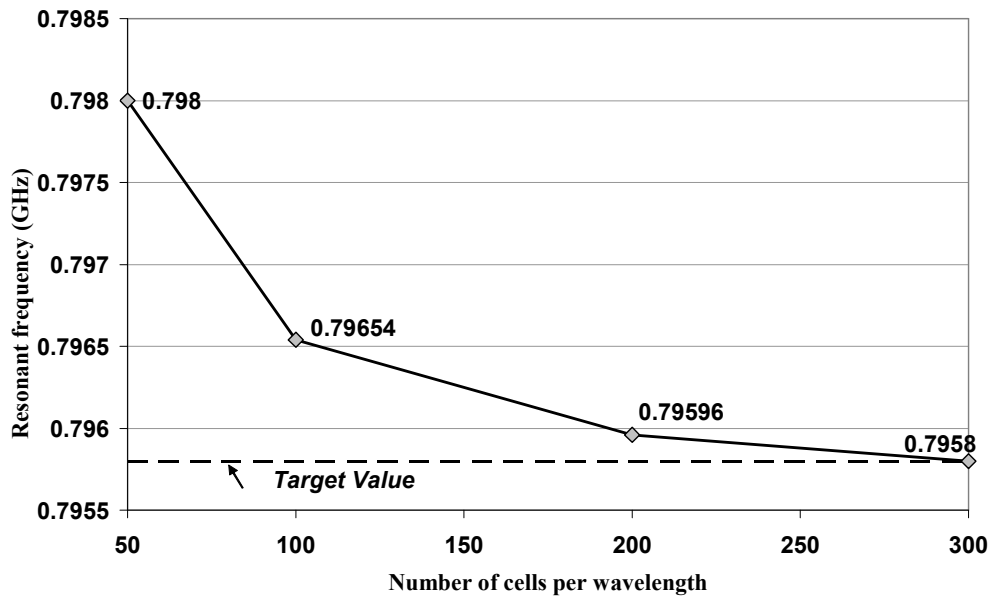


Figure 5.5 Progression of resonant frequency towards target value using ADS “momentum”

variables were the meshing resolution of the model and the resultant resonant frequency. Figure 5.4 demonstrates the influence of meshing resolution on the extraction of the resonant frequency. Each data point is indicative of a simulation performed at a set meshing resolution. As the size of the cells decrease, resulting in a higher meshing resolution, the resonant frequency value generated moves closer to the target value. This target value was the resonant frequency observed in the simulation with ADS during the board design. This model meshing resolution study was performed in a similar fashion using ADS Momentum. The observed resonant frequency also moves toward the target value with each successively higher meshed simulation. Figure 5.5 further supports the importance of model meshing on the resultant generated resonant frequency.

5.3.2 Delta L calculation

The fringing field at the end of the resonator stub is also an important topic that can be examined by modeling with CAD software packages. This fringing field is important because the length of the stub is a critical factor in the characterization of material properties. The length of the resonator is specified as the physical length of the conductor that forms the resonating stub and the additional length generated by the fringing field. This criterion is shown in Figure 5.6. The ADS “schematics” environment was used in a specific example in an effort to confirm the physical computation of the fringing field with the closed form end expression found in Kirschning *et al* [15,27]. The computation of relative permittivity was used as a reference for this part of the experiment. The relative permittivity was entered into the

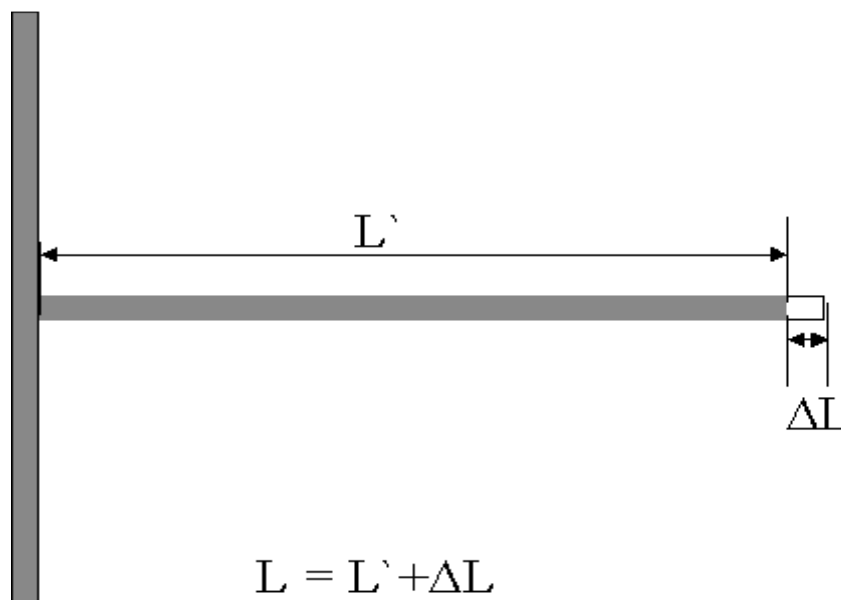


Figure 5.6 Definition of resonator length with consideration of ΔL

Table 5.1 Results of delta L experiment

Determination Method	Relative Permittivity Value	Resonator Length (mil)	Resonant Frequency (GHz)	Computed Delta L (mil)
Schematics using MLOC	9.5	1469.16 (L)	0.795	
Relative permittivity extraction routine	9.5	1461.0 (L')	0.795	7.954 (L'')
Results : $(L \sim = L' + L'') \Rightarrow (L = 1461.0 + 7.954) \Rightarrow (L = 1468.954 \sim = 1469.16)$				

microstrip substrate (MSUB) block in schematics, the length of the resonator (L) was computed, and then the scattering parameter S_{21} was generated. The combination of these parameters were then used with an independently developed relative permittivity calculation algorithm that allowed the determination of the resonant frequency needed to produce the same relative permittivity value as the one used in the schematics model. This relative permittivity value was arrived at with a computation that incorporated the closed form end expression and a computation that did not incorporate the closed form end expression. The results are significant because the microstrip line open circuit (MLOC) symbolic circuit does not account for the end effect. An examination of Table 5.1 validates the closed form end expression given in Kirschning *et al.* The value of the ΔL compensated length generated by the extraction routine is in close proximity to the value given by schematics using MLOC when the resonant frequency and value of relative permittivity are held constant for both methods. The slight difference in final length is due to the variability caused by unknown variables such as the loss tangent of the dielectric and the conductivity of the resonator and groundplane.

5.3.3 Relative permittivity extraction

Figure 5.7 indicates the resonant frequency generated by the 50 ohm resonator model designed to have a first resonance of 800 MHz. This model was simulated using ADS “momentum”. The value calculated using the resultant resonant frequency is within a value of 0.0007 of the target value of 9.5 for relative permittivity. This is significant because the model was created using the value of 9.5 for relative permittivity. The extraction routine uses the variables w (width of resonator), h (height of the substrate), N (number of resonance), L (length of resonator stub), and f_r (resonant frequency) to calculate relative permittivity. The variables w , h , L , and N are assumed to remain the same in the model and in the calculation. The variable f_r is the variable that changes as

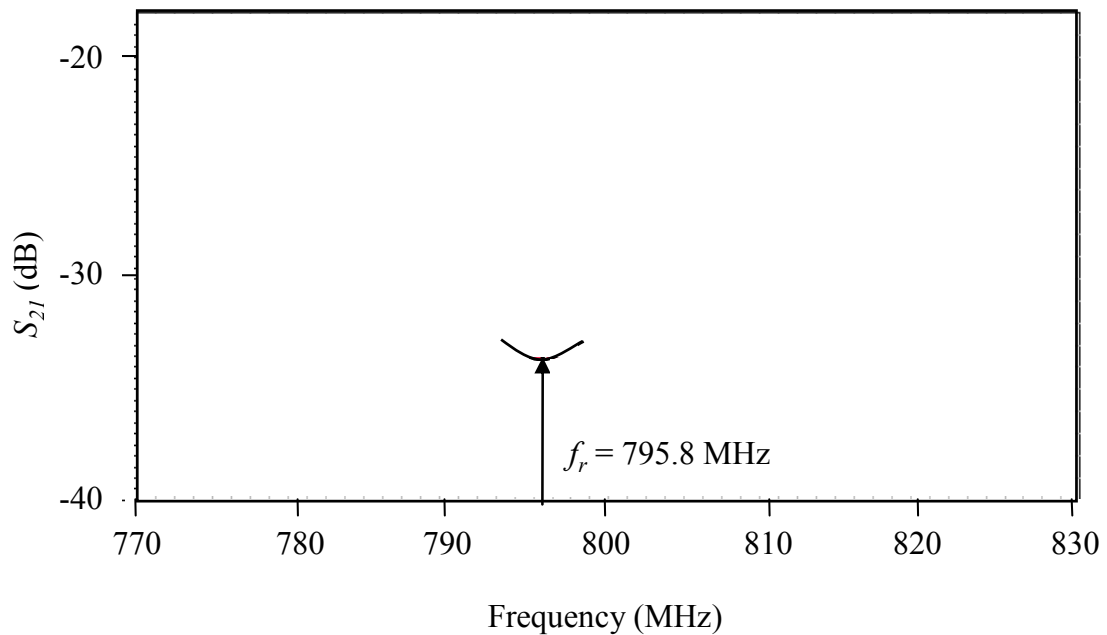


Figure 5.7 Extraction of relative permittivity

Table 5.2 Design parameters for model set

Microstrip Parameters		Stub Parameters		
h	25 mil	Model	w (mil)	L (mil)
ϵ_r	9.5	40 Ω	37.67	1149.21
μ_r	1	50 Ω	24.54	1173.79
σ	5×10^7 S/m	60 Ω	16.3	1193.78
t	0.4 mil	70 Ω	10.89	1210.2
$\tan \delta$	4×10^{-4}	<i>design $N=1=1\text{GHz}$ for all models</i>		

the model simulation changes. The target value for f_r is the value used in the extraction routine to arrive at the calculated value of 9.5 for relative permittivity. This relative permittivity value of 9.5 is also used in the design of the model. Therefore, the goal for confirming the extraction procedure is to arrive at a point of resonance in the model simulation that produces a computed value of relative permittivity that is the same value used in the simulation. It is important to note that this model was created using values for conductivity (1.4×10^7 (S/m)) and loss tangent (2×10^{-4}) that allowed this resonant frequency to be obtained.

A set of models with the design parameters listed in Table 5.2 were developed to further examine the extraction of relative permittivity. These models were meshed at 300, 500, and 700 cells per wavelength. The loss tangent and conductivity values were held constant in all of the performed simulations. The resulting variance in the extracted relative permittivity values can be observed in Table 5.3. Simulating different impedance resonator models shows the deviation from the relative permittivity value used in the

Table 5.3 Extracted relative permittivity and resonant frequency values

300 cells/wavelength		
Z_o	ϵ_r	f_r
70	9.57	0.987
60	9.48	0.991
50	9.39	0.995
40	9.28	1.001
500 cells/wavelength		
Z_o	ϵ_r	f_r
70	9.59	0.986
60	9.48	0.991
50	9.39	0.995
40	9.30	1.000
700 cells/wavelength		
Z_o	ϵ_r	f_r
70	9.59	0.986
60	9.49	0.991
50	9.40	0.995
40	9.30	1.000
<i>model design value $\epsilon_r = 9.5$</i>		

design of the model. It is interesting to note that our extracted value of relative permittivity increases as the impedance of the resonator stub increases.

5.3.4 Sheet resistance and loss tangent extraction

The procedure for the extraction of the dielectric and conductor properties was also performed using ADS “momentum”. In particular, the process for the extraction of loss tangent and sheet resistance was examined. This extraction process was implemented by way of MATLAB coding that was developed based on the technique

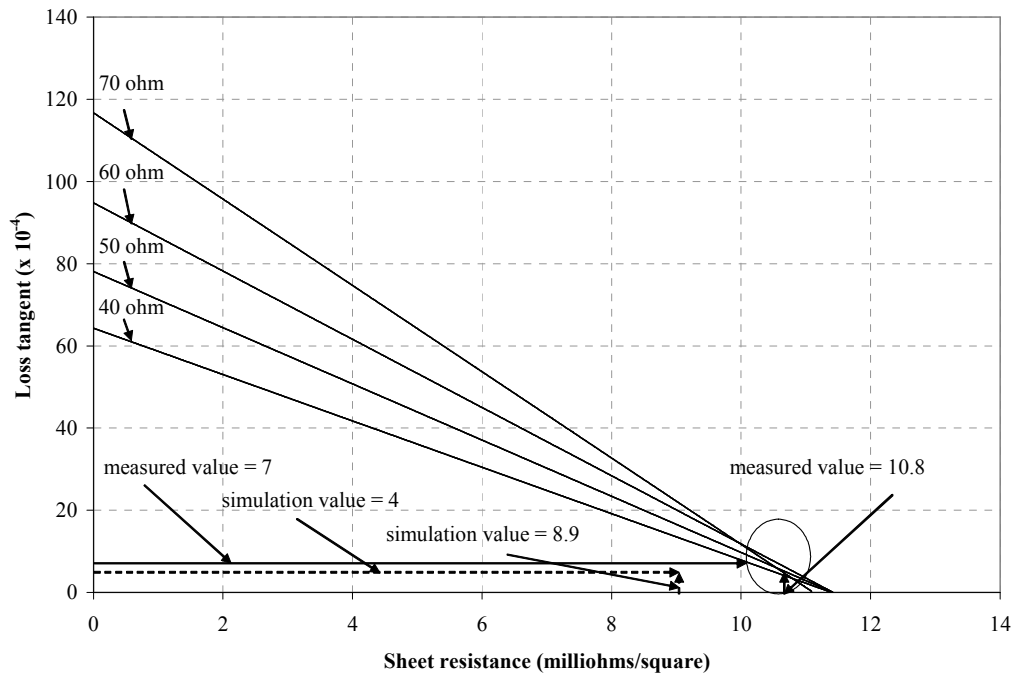


Figure 5.8 300 cells per wavelength sheet resistance vs. loss tangent plot

explained in section 3 of Chapter 2. To accomplish this, 4 models were developed, each producing its own set of data. The design parameters for these models are listed in Table 5.2. The stub parameters indicated were designed for a first resonant frequency ($N=1$) of 1GHz. These models were chosen in order to observe the behavior of the intersection plot routine for the extraction of loss tangent and sheet resistance in terms of symmetry about the 50 Ω characteristic impedance of the thru line. The models were then meshed at resolutions of 300 cells per wavelength, 500 cells per wavelength, and 700 cells per wavelength. Then the models were all simulated to provide the S_{21} versus frequency data necessary to demonstrate the extraction process. This data was then used to form the three sets of intersection plots shown in Figures 5.8, 5.9, and 5.10. This was accomplished by plotting a line representative of all possible combinations of sheet

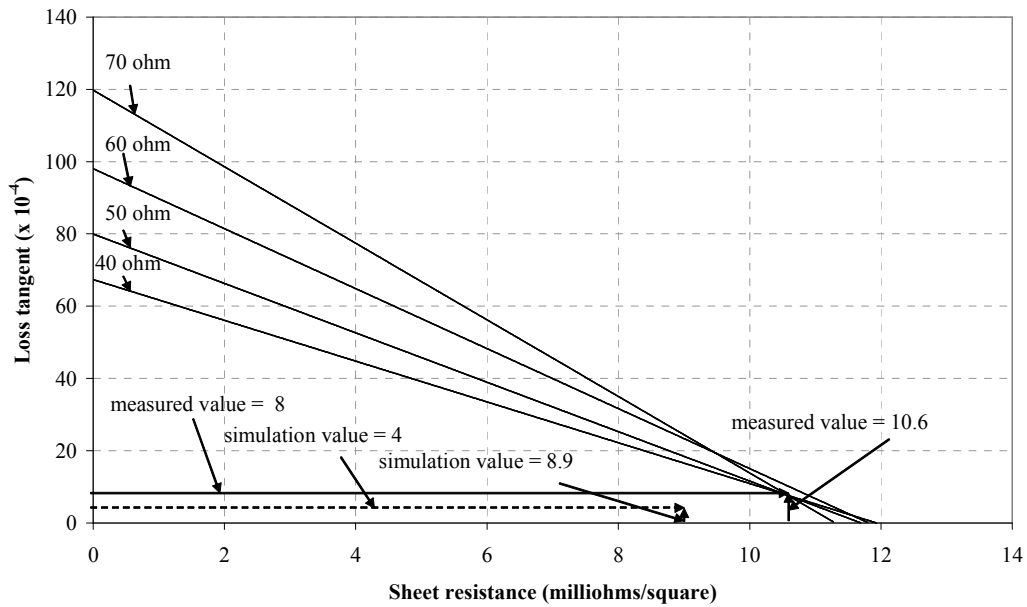


Figure 5.9 500 cells per wavelength sheet resistance vs. loss tangent plot

resistance versus loss tangent for each different impedance model meshed at 300 cells per wavelength. This process was then repeated for the other meshing resolutions. Figures 5.8, 5.9, and 5.10 indicate the intersection plots for the model sets meshed at resolutions of 300, 500, and 700 cells per wavelength, respectively.

A comparison of Figures 5.8, 5.9, and 5.10 indicates that the intersections of the lines for the different impedance lines move towards a single intersection as the resolution of the models increase. This behavior indicates that the extraction of sheet resistance and loss tangent is greatly influenced by the meshing resolution of the model. The target value for R_S indicated in the figures is calculated using (4.1) and the target value for $\tan\delta$ is the value used in the design of the models. The extraction procedure

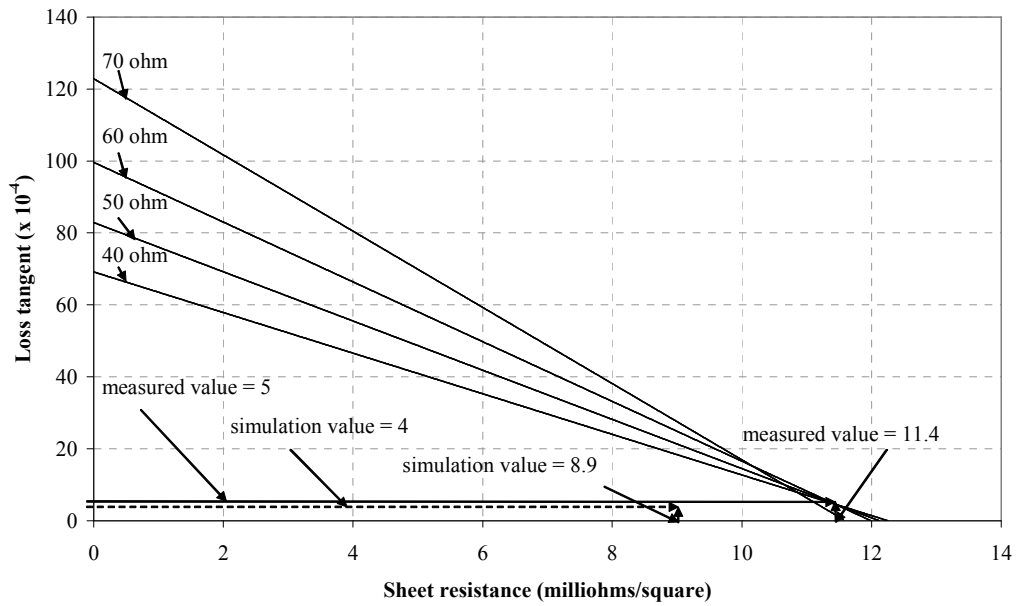


Figure 5.10 700 cells per wavelength sheet resistance vs. loss tangent plot

consistently overestimates R_S while the resultant value for $\tan\delta$ is in close proximity to the value used in the design of the models.

CHAPTER 6

CONCLUSIONS

6.1 Technique summary

A technique for extracting both conductor and dielectric properties using a pair of microstrip tee resonators has been presented. This technique has been demonstrated on transmission lines realized with Ag/Pd conductor on alumina substrate. Characteristic dips in the scattering parameter S_{21} are generated by each tee resonator. These dips can then be used to extract the parameters necessary to compute total attenuation and effective permittivity. This data can then be further used to extract the sheet resistance of the conductor and the loss tangent of the substrate. This effectively defines the properties of the conductor and dielectric that are useful in the design of microwave devices.

A measurement variability study was conducted to estimate the margins of error in data collection. The low variability of same board testing suggests that the measurements process is adequate for the purposes of accurate data collection. The higher variability of board-to-board measurements suggests more variability in the fabrication process than in the measurement process. More test vehicles with tighter fabrication tolerances are desired to ensure that the data collected from measurements is as accurate as possible.

The extracted value of loss tangent for the test board is slightly higher than the value stated in the manufacturer's data sheet while the sheet resistance is expectedly

much greater than that of perfectly smooth copper. Assuming the method is sound, this discrepancy between the expected and extracted loss tangent and sheet resistance values may be a result of board preparation flaws or it could be that the method does not work so well if the conductor loss is much greater than the dielectric loss. It may also be a result of inaccuracies in the equations used, a possibility suggested by the work of Thompson *et al* [30].

6.2 Future work

There is room for improvement in the presented dielectric and conductor extraction process. The equations used for finding the total attenuation and substrate permittivity work reasonably well based on results obtained using both measured and simulated data. The iterative technique and equations used for the extraction of loss tangent and sheet resistance produce results that are reasonably close to expected results. Further investigation into the equations for extracting sheet resistance and loss tangent should be conducted.

Currently the method is being further examined using data measured on a test board with copper etched lines on a microwave laminate substrate. This configuration exhibits a more balanced ratio of conductor and dielectric loss. This is in contrast to the printed Ag/Pd paste on alumina substrate, where the conductor loss was much greater than dielectric loss at our measurement frequencies. Figure 6.1 indicates that the loss tangent and sheet resistance values for the laminate board obtained using the tee resonator approach agree quite favorably with the expected results. More testing on this

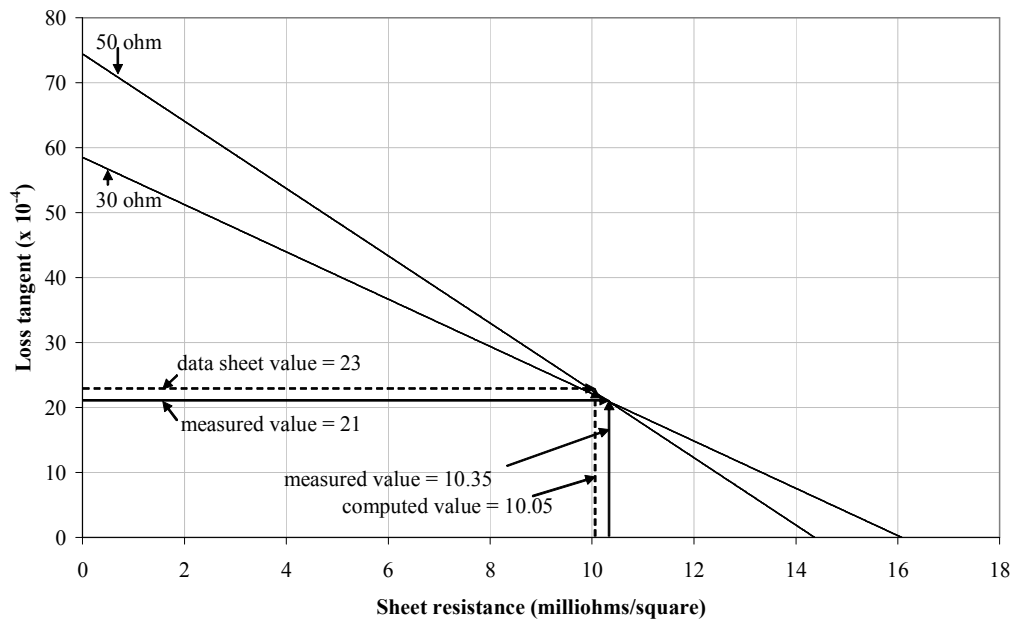


Figure 6.1 Sheet resistance vs. loss tangent plot for test board with copper lines and a microwave laminate substrate

type of configuration should be done as a comparison to the high loss conductor low loss dielectric configuration to determine the limitations of the technique.

The influence of permittivity calculation on the method should be further examined. A trend currently exists whereby the value of extracted relative permittivity increases as the impedance of the resonator stub increases. Accounting for dispersion in the calculation of permittivity could possibly improve the accuracy of the method by eliminating this occurrence. The technique might also benefit from understanding the fringing field at the end of the resonator stub. One way to study this may be to short the end of the half-wavelength resonator stub by way of a via to the groundplane. This would effectively eliminate ΔL from the fringing field. Another way to further study ΔL is by using the common resonances of the long and short resonator pair to extract the

length. These methods would possibly allow a more accurate estimation of delta L. This better understanding of the delta L effect would possibly result in a more accurate extraction of the properties for the conductor and dielectric.

Modeling efforts should also be continued. The modeling of the tee resonators is an effective way to quickly alter parameters of the test vehicle without the burden of fabricating a new test vehicle. Models with high meshing resolutions are needed for the accurate generation of data. These highly meshed models take a great deal of time to simulate due to the large computing requirements. Further work in this area should be conducted to better understand the intricacies of the extraction process.

6.3 Conclusions

The conductor and dielectric properties of microstrip can be extracted using a pair of differing impedance resonators. The technique, however, needs to be further developed to achieve a high level of confidence in the obtained results. The dated equations, limited number of test samples, and imperfect modeling are all areas that should be worked on to improve the extraction technique. The obtainment of a greater set of test samples will allow confidence in the measured data. This will allow a better examination of the equations currently being used. More investment in the time consuming modeling efforts will also help to better understand the strengths and weaknesses of the properties extraction process.

REFERENCES

- [1] E. J. Denlinger, "A Frequency Dependent Solution for Microstrip Transmission Lines", *IEEE Trans. Microwave Theory Tech*, vol. MTT-19, pp. 30-39, Jan. 1971.
- [2] J. D. Woermke, "Soft Substrates Conquer Hard Designs," *Microwaves*, Jan, 1982.
- [3] D. A. Rudy, J. P. Mendelson, and P. J. Munz, "Measurement of RF Dielectric Properties with Series Resonant Microstrip Elements," *Microwave Journal*, Mar. 1998, pp. 22-41.
- [4] J. Carroll, M. Li, and K. Chang, "New Technique to Measure Transmission Line Attenuation," *IEEE Trans. Microwave Theory Tech.*, vol. MTT-43, No. 1, Jan. 1995, pp. 219-222.
- [5] S. M. Wentworth, "Measuring the Microwave Attenuation in Microstrip," *The 31st Southeastern Symposium on System Theory*, Auburn, AL, 1999, pp.200-204.
- [6] D. I. Amey and S. J. Horowitz, "Microwave Material characterization," *ISHM '96 Proc.*, pp. 494-499.
- [7] S. M. Wentworth, *Fundamentals of Electromagnetics with Engineering Applications*, 1st Ed., John Wiley & Sons, Inc., 2005, pp. 502-512.
- [8] D. M. Pozar, *Microwave Engineering*, 2rd Ed., John Wiley & Sons, Inc., 1998, pp. 196-206.
- [9] B. L. Dillaman (1996), *High Frequency Characterization of Materials Used In Hybrid Microelectronic Interconnections and Transmission Lines*. Unpublished master's thesis, Auburn University, Auburn, Alabama.
- [10] R. L. Peterson and R. F. Drayton, "A CPW T-Resonator Technique for Electrical Characterization of Microwave Substrates," *IEEE Microwave and Wireless Components Letters*, Vol. 12, No. 3, March 2002, pp. 90-92.
- [11] E. Belohoubek and E. Denlinger, "Loss Considerations for Microstrip Resonators," *IEEE Trans. Microwave Theory Tech.*, vol. MTT-23, 1975, pp. 522-526.

- [12] E. J. Denlinger, "Radiation from Microstrip Resonators," *IEEE Trans. Microwave Theory Tech.*, vol. MTT-17, pp.235-236, Apr. 1969.
- [13] D. M. Pozar, *Microwave Engineering*, 2rd Ed., John Wiley & Sons, Inc., 1998, pp. 271-275.
- [14] M. N. O. Sadiku, *Elements of Electromagnetics*, 3rd Ed., Oxford University Press, Inc., 2001, pp. 526-527.
- [15] M. Kirschning, R. H. Jansen, and N. H. L. Koster, "Accurate Model for Open End Effect of Microstrip Lines," *Electronics Letters*, Vol. 17, No. 3, 5 February 1981, pp. 123-125.
- [16] D. H. Schrader, *Microstrip Circuit Analysis*, Prentice-Hall, Inc., 1995, p.31
- [17] R. A. Pucel, D. J. Masse and C.P. Hartwig, "Losses in Microstrip," *IEEE Trans. Microwave Theory Tech*, June 1968, pp. 342.
- [18] C. Nguyen, *Analysis Methods for RF, Microwave, and Millimeter-Wave Planar Transmission Line Structures*, John Wiley & Sons, Inc., 2000, pp. 68-70.
- [19] I. J. Bahl, and R. Garg, "Simple and Accurate Formulas for Microstrip with Finite Strip Thickness," *Proc. IEEE*, Vol. 65, 1977, pp. 1611-1612.
- [20] D. M. Pozar, *Microwave Engineering*, 2rd Ed., John Wiley & Sons, Inc., 1998, pp. 163.
- [21] "HP 8510C Network Analyzer: Operating and Programming Manual", 1st ed., Hewlett-Packard, 1991.
- [22] P. B. Johns, "A Symmetrical Condensed Node for the TLM Method," *IEEE Trans. Microwave Theory Tech*, vol. MTT-35, pp.370-377, April, 1987.
- [23] S. Akhtarzad and P. B. Johns, "Three-Dimensional Transmission-Line Matrix Computer Analysis of Microstrip Resonators," *IEEE Trans. Microwave Theory Tech*, vol. MTT-23, pp.990-997, Dec. 1975.
- [24] W. J. Getsinger, "Measurement and Modeling of the Apparent Characteristic Impedance of Microstrip," *IEEE Trans. Microwave Theory Tech*, vol. MTT-31, pp. 624-632, August 1983.
- [25] E. Hammerstad and F. Bekkadal. *Microstrip Handbook*, ELAB Report STF44 A74169, February 1975.
- [26] E. Hammerstad and O. Jensen. "Accurate Models for Microstrip Computer-Aided Design," *MTT Symposium Digest*, 1980.

- [27] M. Kirschning and R. H. Jansen. *Electronics Letters*, January 18, 1982.
- [28] H. A. Wheeler, "Formulas for the Skin Effect," *Proc. IRE*, Vol. 30, September, 1942, pp. 412-424.
- [29] J. C. Rautio, "Microstrip Conductor Loss Models for Electromagnetic Analysis," *IEEE Trans. Microwave Theory Tech*, vol. MTT-51, pp. 915-921, March 2003.
- [30] D.C. Thompson, O. Tantot, H. Jallageas, G.E. Ponchak, M.M. Tentzeris, and J. Papapolymerou, "Characterization of Liquid Crystal Polymer (LCP) Material and Transmission Lines on LCP Substrates from 30 to 110 GHz, " *IEEE Trans Microwave Theory Tech*, vol. MTT-52, pp. 1343-1352. April 2004.

APPENDIX
MATLAB CODE

1 Plot of sheet resistance versus loss tangent code

```
%This program is used to plot two lines for all possible combinations of Sheet  
%Resistance versus Loss Tangent for a pair of tee resonators of different impedances.  
%The intersection point of these two lines indicates the values of loss tangent  
%and sheet resistance.
```

```
%initialize the workspace and set constants
```

```
clc
```

```
clear
```

```
%speed of light
```

```
c=2.998e8;
```

```
%thickness of the substrate
```

```
h=25;
```

```
%thickness of the conductor
```

```
t=0.3937;
```

```
%resonance mode
```

```
N=1;
```

```
%number of points in the vectors
```

```
Np=2000;
```

```
%data for 1st line
```

```
%width of the resonator stub
```

```
w1=25;
```

```
%length of the resonator stub
```

```
L1=1461;
```

```
%calls the function frcompute1.m, returns the resonant frequency
```

```
%(lowest point of S21 dip)
```

```
fr1=frcompute1;
```

```
%calls the function eecompute.m to compute the effective permittivity
```

```
ee1=eecompute(N,L1,fr1,h,w1);
```

```

%calls zcompute.m returns the characteristic impedance of the resonator stub(ohms)
z1=zcompute(ee1,h,t,w1);

%calls the function atcompute1.m, returns total attenuation(dB/in)
at1=atcompute1(ee1,c)

%calls the function ercompute.m, returns relative permittivity
er1=ercompute(N,L1,fr1,h,w1)

%calls the function ar_compute.m, returns radiative attenuation(dB/in)
ar1=ar_compute(c,ee1,fr1,z1,h);

%total attenuation minus radiative attenuation
at_r1=at1-ar1;

%calls the function Rscompute.m, returns the sheet resistance
%NOTE: Initially total attenuation - radiative attenuation is assumed for
%the computation of sheet resistance.
Rsmax1=Rscompute(fr1,w1,h,t,er1,z1,at_r1);

%divides the sheet resistance calculated with the compensated total attenuation
%by the number of specified points
dRs1=Rsmax1/Np;

%forms a vector of values for sheet resistance
%(minimum value=~0 to maximum value=max Sheet resistance)
Rs1=dRs1:dRs1:Rsmax1;

%calls the function accompute.m, returns the conductor attenuation (dB/in)
ac1=acompute(fr1,w1,h,t,er1,z1,Rs1);

%compute dielectric loss by subtracting radiative compensated total loss from
%conductor loss
ad1=at_r1-ac1;

%compute loss tangent as found in Pozar for all possible values
tand1=ad1*c*sqrt(ee1)*(er1-1)/(27.3*er1*(ee1-1)*fr1*.0254);

%data for 2nd line

%width of the resonator stub
w2=61;

%length of the resonator stub
L2=1396;

```

```

%calls the function frcompute2.m, returns the resonant frequency
%(lowest point of S21 dip)
fr2=frcompute2;

%calls the function eecompute.m to compute the effective permittivity
ee2=eecompute(N,L2,fr2,h,w2);

%calls zcompute.m returns the characteristic impedance of the resonator stub(ohms)
z2=zcompute(ee2,h,t,w2);

%calls the function atcompute1.m, returns total attenuation(dB/in)
at2=atcompute2(ee2,c)

%calls the function ercompute.m, returns relative permittivity
er2=ercompute(N,L2,fr2,h,w2)

%calls the function ar_compute.m, returns radiative attenuation(dB/in)
ar2=ar_compute(c,ee2,fr2,z2,h);

%total attenuation minus radiative attenuation
at_r2=at2-ar2;

%calls the function Rscompute.m, returns the sheet resistance
%NOTE: Initially total attenuation - radiative attenuation is assumed for
%the computation of sheet resistance.
Rsm2=Rscompute(fr2,w2,h,t,er2,z2,at_r2);

%divides the sheet resistance calculated with the compensated total attenuation
%by the number of specified points
dRs2=Rsm2/Np;

%forms a vector of values for sheet resistance
%(minimum value= $\sim 0$  to maximum value= $\text{max}$  Sheet resistance)
Rs2=dRs2:dRs2:Rsm2;

%calls the function accompute.m, returns the conductor attenuation (dB/in)
ac2=acompute(fr2,w2,h,t,er2,z2,Rs2);

%compute dielectric loss by subtracting radiative compensated total loss from
%conductor loss.
ad2=at_r2-ac2;

%compute loss tangent as found in Pozar for all possible values
tand2=ad2*c*sqrt(ee2)*(er2-1)/(27.3*er2*(ee2-1)*fr2*.0254);

%plots the two lines that form the intersection point

```

```

plot(Rs1,tand1,Rs2,tand2)
legend('50 ohm','30 ohm')
grid on
xlabel('Rs')
ylabel('tand')

```

2 Code for extracting the resonant frequency for the first line

```

function fr=frcompute1
%This function reads a file containing frequency (GHz)
%versus S21(dB)and returns the resonant frequency.

%loads the file into the variable 'resp'
resp = load('50_avg.txt');

%determines the number of values in the file
s = size(resp);

%vector used to index through the values in the columns
%of the text(data) file
m = (1:s(1));

%finds the lowest value in the S21(dB) column
[min_dB,i] = min(resp);

%designates the corresponding frequency as the
%resonant frequency
fr = resp(i(2));

%converts frequency in GHz to Hz
fr =fr* 1e9;

```

3 Effective permittivity calculation code

```

function ee=eecompute(N,L,fr,h,w)
%effective permittivity calculation

% This program is used to perform the extraction of effective permittivity
% given the necessary values of N(mode number), L(length of resonator stub),
% F(the operating frequency of the corresponding mode number N, h(height of
% substrate), and w(width of the resonator).
%
% You must have the functions improved_er, and Lcorrect in the same
% working directory to use this program.

```

```

%
% The program will compute a converged value of effective permittivity with the
% inclusion of a calculated value for the additional length of the resonator stub
% created by the fringing fields at the end of the stub.
%
% Note: the values stabilize after the second loop through, therefore the final
% value is assumed the adequately compensated value.

%Constants to be used throughout the program, converts
% mils to meters
c = 2.998e8;
L_m = L*25.4e-6;
h_m = h*25.4e-6;
w_m = w*25.4e-6;

%Calculate the effective permittivity of tee resonator
e_eff = (((2*N-1)*c)/(4*fr*L_m))^2;

%functions that perform the extraction of er
er_i = improved_er(e_eff,h_m,w_m);
delL = Lcorrect(w_m,h_m,er_i,e_eff);

e_eff2 = (((2*N-1)*c)/(4*fr*(L_m+delL)))^2;
e_eff = e_eff2;
er_i2 = improved_er(e_eff,h_m,w_m);
er_i = er_i2;
delL2 = Lcorrect(w_m,h_m,er_i,e_eff);

e_eff3 = (((2*N-1)*c)/(4*fr*(L_m+delL2)))^2;
e_eff = e_eff3;
er_i3 = improved_er(e_eff,h_m,w_m);
er_i = er_i3;
delL3 = Lcorrect(w_m,h_m,er_i,e_eff);

%This is the last necessary loop for the convergence of the final value
e_eff4 = (((2*N-1)*c)/(4*fr*(L_m+delL3)))^2;
e_eff = e_eff4;
er_i4 = improved_er(e_eff,h_m,w_m);
er_i = er_i4;
delL4 = Lcorrect(w_m,h_m,er_i,e_eff);

ee=e_eff;

```

4 Characteristic impedance calculation code

```
function z_o = zcompute(ee,h,t,w)

%This function computes the characteristic impedance
%for a particular resonator stub.

%Computing the effective width "we"
if (w/h)<=(1/(2*pi))
    we=w+((1.25*t)/pi)*(1+log((4*pi*w)/t));
end
if (w/h)>=(1/(2*pi))
    we=w+((1.25*t)/pi)*(1+log((2*h)/t));
end

%computing the characteristic impedance "z_o"
if (w/h)<=1
    z_o=(60/sqrt(ee))*log((8*h)/we+0.25*(we/h));
end
if (w/h)>=1
    z_o=((120*pi)/sqrt(ee))*(we/h+1.393+0.667*log(we/h+1.444))^-1;
end

z_o=z_o
```

5 Code for calculating total attenuation for the first line

```
function at = atcompute1(ee,c)
%This function reads a file containing frequency (GHz)
%versus S21(dB)and returns the total attenuation (dB/in).

%loads the file into the variable 'resp'
resp = load('50_avg.txt');

%determines the number of values in the file
s = size(resp);

%vector used to index through the values in the columns
%of the text(data) file
m = (1:s(1));

%finds the lowest value in the S21(dB) column
[min_dB,i] = min(resp(m,2));
```

```

%designates the corresponding frequency as the
%resonant frequency
f_res = resp(i,1)

%determines the 3dB value used to find the
%corresponding frequency for the computation
%of the 3dB bandwidth
three_dB = min_dB+3;

%finds the S21 values that correspond to the 3dB
%bandwidth limits(upper frequency and lower frequency)
span = find(resp(m,2) <= three_dB);

%sets the upper and lower limit frequencies found
%from the step directly above into variables
%lower limits
x2 = resp(min(span),2);
y2 = resp(min(span),1);

%upper limits
xx2 = resp(max(span),2);
yy2 = resp(max(span),1);

%find lower value just past the <= three_dB point
x1 = resp(min(span)-1,2);
y1 = resp(min(span)-1,1);

%find upper value just past the <= three_dB point
xx1 = resp(max(span)+1,2);
yy1 = resp(max(span)+1,1);

%perform the linear interpolation
y_low = y1+(y2-y1)*((three_dB-x1)/(x2-x1));
y_high = yy1+(yy2-yy1)*((three_dB-xx1)/(xx2-xx1));

%computes the 3dB bandwidth by subtracting the corresponding
%frequency values of the upper and lower S21 3dB limits respectively
BW = y_high-y_low;

%computes the loaded quality factor
QL = f_res/BW;
%intermediate step
T=1-2*10^(min_dB/10);

%calculate the unloaded Q
Qu=QL/sqrt(T);

```

```
%computes f_res in Ghz to f_res in Hz
fr=f_res*1e9;
```

```
%total attenuation calculated in dB/in
at=(8.686*pi*fr*sqrt(epsilon))/(c*Qu*39.37)
```

6 Relative permittivity calculation code

```
function er=ercompute(N,L,fr,h,w)
%relative permittivity calculation

% This program is used to perform the extraction of relative permittivity
% given the necessary values of N(mode number), L(length of resonator stub),
% F(the operating frequency of the corresponding mode number N, h(height of
% substrate), and w(width of the resonator).
%
% You must have the functions improved_er, and Lcorrect in the same
% working directory to use this program.
%
% The program will compute a converged value of relative permittivity with the
% inclusion of a calculated value for the additional length of the resonator stub
% created by the fringing fields at the end of the stub.
%
% Note: the values stabilize after the second loop through, therefore the final
% value is assumed the adequately compensated value.

%Constants to be used throughout the program, converts
%inches to meters
c = 2.998e8;
L_m = L*25.4e-6;
h_m = h*25.4e-6;
w_m = w*25.4e-6;

%Calculate the effective permittivity of t resonator
e_eff = (((2*N-1)*c)/(4*fr*L_m))^2;

%functions that perform the extraction of er
er_i = improved_er(e_eff,h_m,w_m);
delL = Lcorrect(w_m,h_m,er_i,e_eff);

e_eff2 = (((2*N-1)*c)/(4*fr*(L_m+delL)))^2;
e_eff = e_eff2;
er_i2 = improved_er(e_eff,h_m,w_m);
er_i = er_i2;
```

```

delL2 = Lcorrect(w_m,h_m,er_i,e_eff);

e_eff3 = (((2*N-1)*c)/(4*fr*(L_m+delL2)))^2;
e_eff = e_eff3;
er_i3 = improved_er(e_eff,h_m,w_m);
er_i = er_i3;
delL3 = Lcorrect(w_m,h_m,er_i,e_eff);

%This is the last necessary loop for the convergence of the final value
e_eff4 = (((2*N-1)*c)/(4*fr*(L_m+delL3)))^2
e_eff = e_eff4;
er_i4 = improved_er(e_eff,h_m,w_m)
er_i = er_i4;
delL4 = Lcorrect(w_m,h_m,er_i,e_eff);

er=er_i;

```

7 Code used in the permittivity calculation

```

function y = improved_er(e_eff,h_m,w_m)
%Perform iteration to determine relative permittivity (e_r).

%Create a vector representing possible values for the relative permittivity constant.
n = linspace(0.0, 20.0, 100000);

%Loop that performs the actual extraction.
for(x = 1:1:100000)
    b = 0.564*((n(x)-0.9)/(n(x)+3))^0.053;
    a =
    1+(1/49)*log(((w_m/h_m)^4+(w_m/(52*h_m)^2))/((w_m/h_m)^4+0.432))+(1/18.7)*log
    (1+(w_m/(18.1*h_m)))^3;
    e_trial = ((n(x)+1)/2)+((n(x)-1)/2)*(1+10*(h_m/w_m))^(a*b);
    if (e_trial >= e_eff)
        break
    end
end
%value of relative permittivity
y = n(x);

```

8. Code used to compute ΔL

```

function y = Lcorrect(w_m,h_m,er_i,e_eff)

```

%This function computes the length added to the physical
 %length of the microstrip tee resonator due to fringing fields.
 %Uses Kirschning et al in Elect. Letters, Feb 5, 1981 Vol 17, No.3, p.123

```
E1 = 0.434907*((e_eff^.81+0.26)/(e_eff^.81-
.189))*(((w_m/h_m)^0.8544+0.236)/((w_m/h_m)^.8544+.87));
E2 = 1+(((w_m/h_m)^0.371)/(2.358*er_i+1));
E3 = 1+(((0.5274*atan(0.084*(w_m/h_m)^(1.9413/E2)))/e_eff^0.9236);
E4 = 1 + 0.0377*atan(0.067*(w_m/h_m)^1.456)*(6-5*exp(0.036*(1-er_i)));
E5 = 1-.218*exp(-7.5*(w_m/h_m));
y = ((E1*E3*E5)/E4)*h_m;
```

9 Code for the calculation of attenuation due to radiation

```
function ar=ar_compute(c,ee,fr,z,h)
%This function is used to compute radiative losses in dB/in.

%Converts height in mil to height in meters
h_m=h*25.4e-6;

%Computing the constant R
R=((ee+1)/ee)-((ee-1)^2/(2*ee^(3/2)))*log((sqrt(ee)+1)/(sqrt(ee)-1));

%Computing the radiation loss in dB/in
ar=(8.686*pi*h_m^2*R*fr^3)/(z*c^3*39.37)
```

10 Sheet resistance calculation code

```
function Rs=Rscompute (fr,w,h,t,er,z,ac)
%Function calculates sheet resistance for microstrip.
%w(stub width), h(substrate height), & t(conductor thickness)
%are in units of mil.
%x1-x5 are temporary variables.

%conductivity
sigma=5e7;

%calculate an initial value for Rs (ohms/square)
Rs_i=sqrt((pi*4*pi*10^(-7)*fr)/sigma)

%calculate the effective line width
x1=(t/h)*(coth(sqrt(6.517*w/h)))^2;
```

```

dwp=(t/pi)*(log(1+10.8731/x1));
dw=(dwp/2)*(1+1/cos(h*(sqrt(er-1))));
we=w+dw;

%calculate some temporary constants
x2=1+(h/we)+(h/(pi*we))*(log(2*h/t)-(t/h));
x3=1-(we/(4*h))^2;
x4=((we/h)+(2/pi)*log(2*pi*2.7183*((we/(2*h))+0.94)))^-2;
x5=(we/h)+(we/(pi*h))/((we/(2*h))+0.94);
x6=1+(h/we)+(h/(pi*we))*(log((4*pi*w)/t)+(t/w));

%convert alpha c form dB/in to dB/mil
acmil=ac/1000;

%calculate sheet resistance
if (w/h)>(1/(2*pi))
    if (we/h)<=2
        Rs=acmil/((8.686/(2*pi*z*h))*x3*x2);
    else if (w/h)>2
        Rs=acmil/((8.686/(z*h))*x2*x5*x4);
    end
end
else if (w/h)<(1/(2*pi))
    Rs=acmil/(((8.686/(2*pi*z*h))*x3*x6));
end
end
end

```

11 Conductor attenuation calculation code

```

function ac=acompute(fr,w,h,t,er,z,Rs)
%Function calculates conductor attenuation(dB/in).
%w(stub width), h(substrate height), & t(conductor thickness)
%are in units of mil.
%x1-x5 are temporary variables.

%conductivity
sigma=5e7;
%calculate an intial value for Rs (ohms/square)
Rs_i=sqrt((pi*4*pi*10^(-7)*fr)/sigma)

%calculate the effective line width
x1=(t/h)*(coth(sqrt(6.517*w/h)))^2;
dwp=(t/pi)*(log(1+10.8731/x1));
dw=(dwp/2)*(1+1/cos(h*(sqrt(er-1))));

```

```

we=w+dw;

%calculate some temporary constants
x2=1+(h/we)+(h/(pi*we))*(log(2*h/t)-t/w);
x3=1-(we/(4*h))^2;
x4=((we/h)+(2/pi)*log(2*pi*2.7183*(((we/(2*h))+0.94))))^-2;
x5=(we/h)+(we/(pi*h))/((we/(2*h))+0.94);
x6=1+(h/we)+(h/(pi*we))*(log(4*pi*w/t)+(t/w));

%calculate alpha c
if (w/h)>(1/(2*pi))
    if (w/h)<=2
        ac=(8.686*Rs/(2*pi*z*h))*x3*x2;
    else if (w/h)>2
        ac=(8.686*Rs/(z*h))*x2*x5*x4;
    end
end
else if (w/h)<=(1/(2*pi))

    ac=((8.686*Rs/(2*pi*z*h))*x3*x6);
end
end

%converts from (dB/mil) to (dB/in)
ac=ac*1000;

```

12 Code for extracting the resonant frequency for the second line

```

function fr=frcompute2
%This function reads a file containing frequency (GHz)
%versus S21(dB)and returns the resonant frequency.

%loads the file into the variable 'resp'
resp = load('30_avg.txt');

%determines the number of values in the file
s = size(resp);
%vector used to index through the values in the columns
%of the text(data) file
m = (1:s(1));

%finds the lowest value in the S21(dB) column
[min_dB,i] = min(resp);

```

```
%designates the corresponding frequency as the  
%resonant frequency  
fr = resp(i(2));
```

```
%converts frequency in GHz to Hz  
fr =fr*1e9;
```

13 Code for calculating total attenuation for the second line

```
function at = atcompute2(ee,c)  
%This function reads a file containing frequency (GHz)  
%versus S21(dB)and returns the total attenuation (dB/in).
```

```
%loads the file into the variable 'resp'  
resp = load('30_avg.txt');
```

```
%determines the number of values in the file  
s = size(resp);
```

```
%vector used to index through the values in the columns  
%of the text(data) file  
m = (1:s(1));
```

```
%finds the lowest value in the S21(dB) column  
[min_dB,i] = min(resp(m,2));
```

```
%designates the corresponding frequency as the  
%resonant frequency  
f_res = resp(i,1)
```

```
%determines the 3dB value used to find the  
%corresponding frequency for the computation  
%of the 3dB bandwidth  
three_dB = min_dB+3;
```

```
%finds the S21 values that correspond to the 3dB  
%bandwidth limits(upper frequency and lower frequency)  
span = find(resp(m,2) <= three_dB);
```

```
%sets the upper and lower limit frequencies found  
%from the step directly above into variables  
%lower limits  
x2 = resp(min(span),2);  
y2 = resp(min(span),1);
```

```

%upper limits
xx2 = resp(max(span),2);
yy2 = resp(max(span),1);

%find lower value just past the <= three_dB point
x1 = resp(min(span)-1,2);
y1 = resp(min(span)-1,1);

%find upper value just past the <= three_dB point
xx1 = resp(max(span)+1,2);
yy1 = resp(max(span)+1,1);

%perform the linear interpolation
y_low = y1+(y2-y1)*((three_dB-x1)/(x2-x1));
y_high = yy1+(yy2-yy1)*((three_dB-xx1)/(xx2-xx1));

%computes the 3dB bandwidth by subtracting the corresponding
%frequency values of the upper and lower S21 3dB limits respectively
BW = y_high-y_low;

%Computes the loaded quality factor
QL = f_res/BW;

%intermediate step
T=1-2*10^(min_dB/10);

%calculate the unloaded Q
Qu=QL/sqrt(T);

%computes f_res in Ghz to f_res in Hz
fr=f_res*1e9;

%total attenuation calculated in dB/in
at=(8.686*pi*fr*sqrt(epsilon))/(c*Qu*39.37)

```